SANDIA REPORT
SAND2021-9854
Printed August 2021
Unlimited Release

Sandia National Laboratories

Fire-Induced Pressure Response and Failure Characterization of PCV/SCV/3013 Containers – Phase 3

Hector Mendoza, Walt Gill, Austin Baird, Victor Figueroa, James McClard*, Ray Sprankle*, Steve Hensel*, Danielle Michel, and Shane Adee.

*Collaborators from Savannah River Site

Prepared by
Sandia National Laboratories
Albuquerque, New Mexico
87185 and Livermore,
California 94550

Issued by Sandia National Laboratories, operated for the United States Department of Energy by National Technology & Engineering Solutions of Sandia, LLC.

Available to DOE and DOE contractors from
U.S. Department of Energy
Office of Scientific and Technical Information
P.O. Box 62
Oak Ridge, TN 37831

Telephone: (865) 576-8401
Facsimile: (865) 576-5728
E-Mail: reports@osti.gov
Online ordering: http://www.osti.gov/scitech

Available to the public from
U.S. Department of Commerce
National Technical Information Service
5301 Shawnee Rd
Alexandria, VA 22312

Telephone: (800) 553-6847
Facsimile: (703) 605-6900
E-Mail: orders@ntis.gov
Online order: https://classic.ntis.gov/help/order-methods/

ABSTRACT

Several Department of Energy (DOE) facilities have materials stored in robust, welded, stainless-steel containers with presumed fire-induced pressure response behaviors. Lack of test data related to fire exposure requires conservative safety analysis assumptions for container response at these facilities. This conservatism can in turn result in the implementation of challenging operational restrictions with costly nuclear safety controls. To help address this issue for sites that store DOE 3013 stainless-steel containers, a series of ten tests were undertaken at Sandia National Laboratories. The goal of this test series was to obtain the response behavior for various configurations of DOE 3013 containers with various payload compositions when exposed to one of two ASTM fire conditions. Key parameters measured in the test series included identification of failure-specific characteristics such as pressure, temperature, and whether or not a vessel was breached during a test. Numerous failure-specific characteristics were identified from the ten tests. This report describes the implementation and execution of the test series performed to identify these failure-specific characteristics. Discussions on the test configurations, payload compositions, thermal insults, and experimental setups are presented. Test results in terms of pressurization and vessel breach (or no-breach) are presented along with corresponding discussions for each test.

ACKNOWLEDGEMENTS

This work was funded by SRNS/NNSA IEW 4375203013 Container Fire-Induced Pressure Response and Failure Characterization. The authors of this paper would like to thank Vincent Valdez, Alvaro Agusto Cruz-Cabrera, Ryan Flanagan, Edward Bystrom, Kelly Urvanejo, Travis Fitch, June Stanley, Brandon Servantes, Donald Mcmanaway, Jason Goar, Enrico Quintana, Jason Brown, Raymond Fuentes, Danny B. Williams, Carissa A. Grey, Doug Ammerman, and the whole team for their help with test executions. We also thank Ethan Zepper for peer reviewing this document.

This paper describes objective technical results and analysis. Any subjective views or opinions that might be expressed in the paper do not necessarily represent the views of the U.S. Department of Energy or the United States Government.

Sandia National Laboratories is a multi-mission laboratory managed and operated by National Technology & Engineering Solutions of Sandia, LLC, a wholly owned subsidiary of Honeywell International Inc., for the U.S. Department of Energy's National Nuclear Security Administration under contract DE-NA0003525.

This manuscript has been authored in collaboration with Savannah River Nuclear Solutions, LLC under Contract No. DE-AC09-08SR22470 with the U.S. Department of Energy. The United States Government retains a non-exclusive, paid-up, irrevocable, worldwide license to publish or reproduce the published form of this work, or allow others to do so, for United States Government purposes.

CONTENTS

LIST OF FIGURES

LIST OF TABLES

This page left blank

ACRONYMS AND DEFINITIONS

Abbreviation	Definition
ARF	Airborne Release Fraction
ASTM	American Society for Testing and Materials
BTCC	Bagless Transfer Convenience Can
BTIC	Bagless Transfer Inner Container
DOE	Department of Energy
DOE-EM	DOE's office of Environmental Management
DOT	Department of Transportation
EPD	Engineered Products Division
FEA	Finite Element Analysis
FLAME	Fire Laboratory for Accreditation of Models and Experiments
HAC	Hypothetical Accident Conditions
LANL	Los Alamos National Laboratories
MIDAS	Mobile Instrumentation Data Acquisition System
NQA	Nuclear Quality Assurance
NNSA	National Nuclear Security Administration
RF	Respirable Fraction
SNL	Sandia National Laboratories
SRNS	Savannah River Nuclear Solutions
SRS	Savannah River Site
TC	Thermocouple
TRU	Transuranic
TTC	Thermal Test Complex
WIPP	Waste Isolation Pilot Plant

1. INTRODUCTION

Many Department of Energy (DOE) facilities have materials stored in containers with presumed fire-induced pressure response behaviors. These pressure response behaviors can influence characterizing parameters, including the Airborne Release Fraction (ARF). The ARF is a coefficient used to estimate the fraction of a material within a container that can escape and be suspended in the surrounding air and made available for airborne transport under a specific set of induced physical stresses [1]. This coefficient is used by nuclear storage facilities where material (e.g., mixed waste) is stored in containers, and many ARF calculations are a function of the maximum pressure realized by a container. Due to the lack of test data related to fire exposure, overly conservative release pressures are assumed for container response at some facilities for nuclear safety. These assumptions, however, can result in overly conservative dose estimates that require challenging operational restrictions with expensive nuclear safety controls. The DOE 3013 container is one of these containers currently operating with conservative safety assumptions. Obtaining more realistic pressure response and container failure information can help reduce control complexity (and therefore cost) to the DOE complex. Consequently, measuring vessel response when a 3013 container is breached are characteristics of significant importance for this test campaign, particularly because of the dependence of ARFs on the maximum pressure realized by a container.

DOE 3013 containers are normally nested inside primary and secondary containment vessels (PCVs and SCVs, respectively) in 9975 shipping packages, as shown in Figure 1-1. 9975s provide substantial protection of inner contents within a fire. However, when removed from the 9975, the SCV and inner containers could produce high-pressure releases during direct fire events. The DOE 3013 container itself is a nested package of three containers that are used to store material. The 3013 assembly typically consists of: (1) a welded outer 3013 container, (2) a welded inner 3013 container, and (3) a vented inner-most container called the convenience can which contains the payload. The convenience can and inner container isolate the contents and assure that the outer container can be maintained free of material contamination during welding. The outer container provides a Safety Class pressure boundary to prevent release of any contents [2]. Two versions of the outer 3013 containers were considered in this test series that are distinguished by variations in their manufacturing process; a flow-formed outer container produced by Dynamic Flowform (the *ARIES Flowform Set Long Term Storage Assembly,* referred to as simply the "Flowform" version in the remainder of this report), and a machined outer 3013 container produced by Westinghouse Engineered Products Division (the *EPD Set 3013 Package Assembly*, referred to as simply the "EPD" version in the remainder of this report).

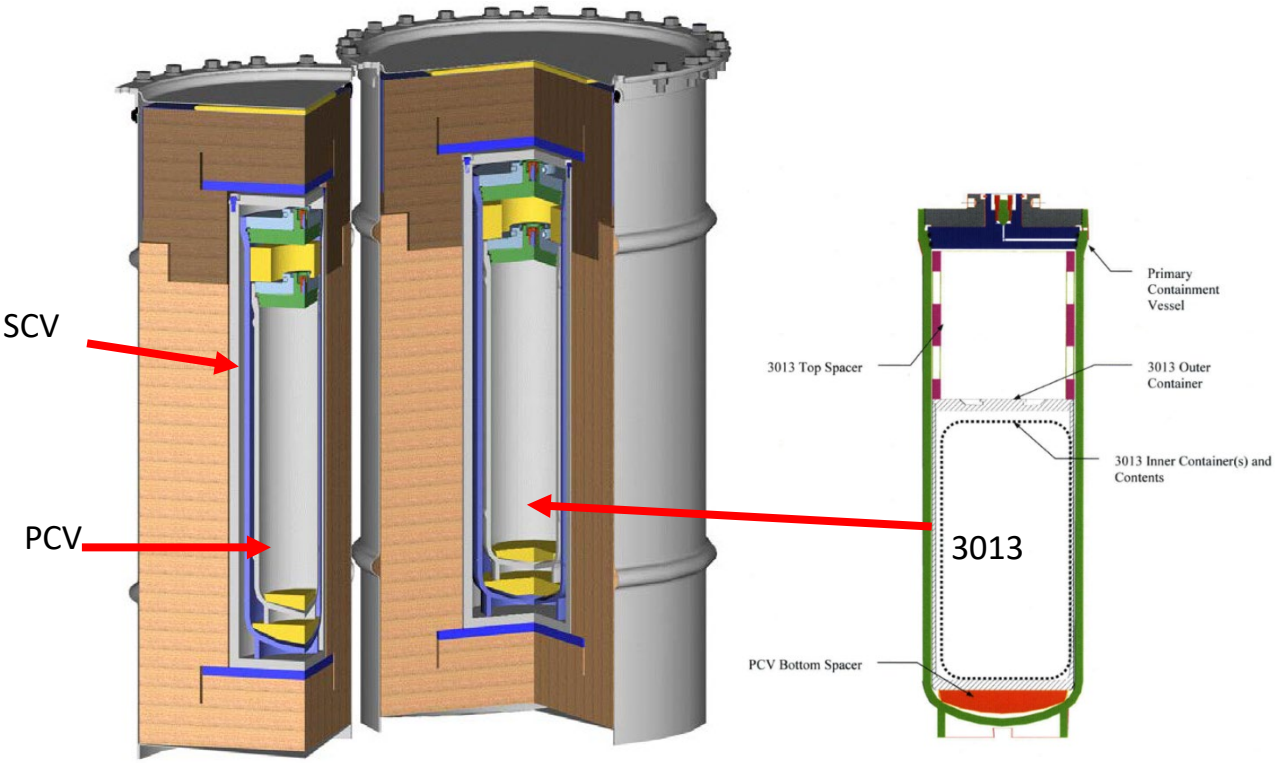

Figure 1-1. 9975 Package showing the 3013 container nested inside a primary containment vessel (PCV), which is nested inside a secondary containment vessel (SCV).

The fire response behavior of the 3013 containers capturing bounding conditions has not been previously assessed. Therefore, Sandia National Laboratories (SNL) and Savannah River Site (SRS) carried out a test campaign to characterize the pressure response behavior for the two versions of the DOE-STD-3013 container when filled with a surrogate payload and exposed to a relevant fire environment. Specifically, this test campaign aimed to determine whether the container will fail under bounding fire conditions. As part of the failure characterization, the campaign aimed to measure and identify failure specific characteristics that consist of: (1) the container pressure response throughout a test, (2) the evolution of container temperature throughout a test, and (3) failure type if the vessels fail during a test. Variations in thermal insult and payload composition (consisting of bounding amounts of moisture and added salts) were considered in this test series in an attempt to comprehensively understand the vessel response in fire scenarios. These characteristics intend to inform future estimates of the Airborne Release Fraction/Respirable Fraction (ARF/RF).

The test campaign described in this report is part of a larger series that also includes fire testing of the primary containment vessel (PCV) and the secondary containment vessel (SCV) of the 9975 shipping package, which respectively corresponded to Phase 1 and Phase 2 of the full series. Phase 1, which helped identify conservative test orientations for test subjects in the full test series, was carried out in 2018/2019 between SNL and SRS. Phase 2 has not been carried out up to this point,

but part of the scope of Phase 2 was addressed during Phase 1. Phase 3, which targets the fire-induced pressure response of the 3013 container under bounding conditions (thermal insult and expected variations in payload), is the focus of this report. The remainder of this report discusses the details of the Phase 3 test campaign carried out by SNL and SRS in the winter of 2020/2021 at the SNL Thermal Test Complex. Section 2 describes the test setups used and includes further details on the preparation and differences between the two 3013 container versions. The heating profiles used to provide the thermal insult are also described in Section 2. The test matrix for this test campaign is described in Section 3, and the results and discussion of the tests carried out are described in Section 4. This report ends with a summary of the Phase 3 test campaign in Section 5.

2. TEST SETUPS

The tests discussed in this report were executed according to the test plan prepared by SNL for this test campaign; *PCV/SCV/3013 Thermal Test Program Phase 3 Test Plan Rev. 0* [3]. A total of 10 tests were executed using the same test setup, where the vessels were tested in a horizontal orientation. This chosen orientation was based on Phase 1 of the PCV/SCV/3013 test program, where thermal testing identified a horizontal orientation as the most conservative scenario for primary containment vessels (PCVs) of the 9975 shipping package [4]. While the test configurations were the same in the tests discussed here, the tests varied by either (1) the heating profile imposed on the vessel, (2) the vessel payload composition, or (3) the version of the outer 3013 container.

The subsections below outline the details of how this test campaign was executed: Section 2.1 discusses the test units and their corresponding payloads; Section 2.2 discusses the diagnostics of interest and the instrumentation used on the vessels; Section 2.3 discusses the heater setups and test configurations; and Section 2.4 discusses the heating profiles used in this test campaign.

2.1. Preparation of Test Subjects

All test units were constructed and prepared at Los Alamos National Laboratory (LANL) under an NQA-1 quality assurance program documented in *LANL Phase 3 Container Loading in Support of the Fire-Induced Pressure Response and Failure Characterization of PCV/SCV/3013 Containers* [5]. Details of the test units and the payload are discussed below in three parts: (1) overview of the test units, modifications to test units, and the payload of the test units.

2.1.1. Test Units

While the Flowform and EPD outer containers have roughly the same dimensions, tolerances, and minimum inner volume, the containers have structural variations due to their different manufacturing processes. In particular, the containers manufactured by the flow-form process have higher residual stresses and tensile strength due to the cold work manufacturing process [5]. Furthermore, the inner containers and convenience cans that complete the 3013 container-set also vary for each configuration. Cross-sectional drawings for the Flowform and EPD container sets are respectively captured in Figure 2-1 and Figure 2-2. The EPD set was completed with a Hanford Bagless Transfer Inner Container (BTIC) while the Flowform set was completed with an ARIES inner container. For the convenience can, the EPD set was completed with a Hanford Bagless Transfer Convenience Can (BTCC). The dimensions of this convenience can required a stainless-steel disk placed inside to conservatively minimize the unoccupied free volume given the payload amount considered in these studies (since pressurization is sensitive to free volume, free volume was minimized only to the point where bounding case was still captured) [5]. In the Flowform set, a shorter version of the Cogema convenience can was used, so an additional stainless-steel disk was placed externally, in between the convenience can and the inner container. It should be noted that, other than being required to be vented (allowing gas leakage), the design of the convenience can of each configuration is not specified by DOE-STD-3013, but it is required to be present. The convenience can inside the EPD set has a filtered vent that allows significant gas flow while the Cogema can inside the Flowform set is double-crimped (like a food can) but without an elastomeric seal, so while gas escapes the can, the flow rate is much lower than for the EPD convenience can. Although the inner container is required to be welded, it is not a Safety Class vessel, so it was decided that a hole would be drilled in the tested inner containers to simulate a failed container and to directly expose the outer container to the gases generated during the test. Ultimately, however, the vessel under test for this campaign was the outer container because; (1) it provides the pressure

boundary to prevent release of any contents, (2) it is the only container from the assembly that is credited in safety basis, and per DOE-STD-3013 it is considered "Safety Class" (SC) for normal storage conditions [6], and (3) the inner container was modified with a perforation.

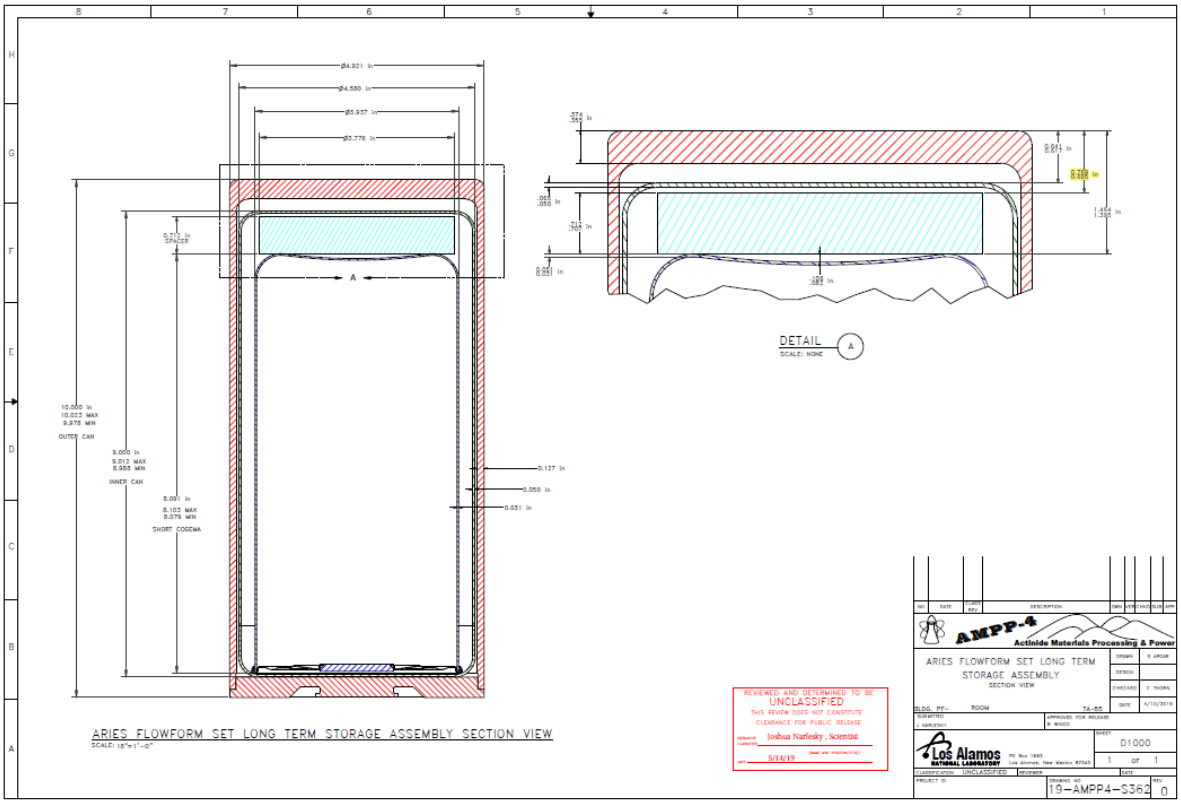

Figure 2-1. Cross-sectional drawing of the Flowform assembly version.

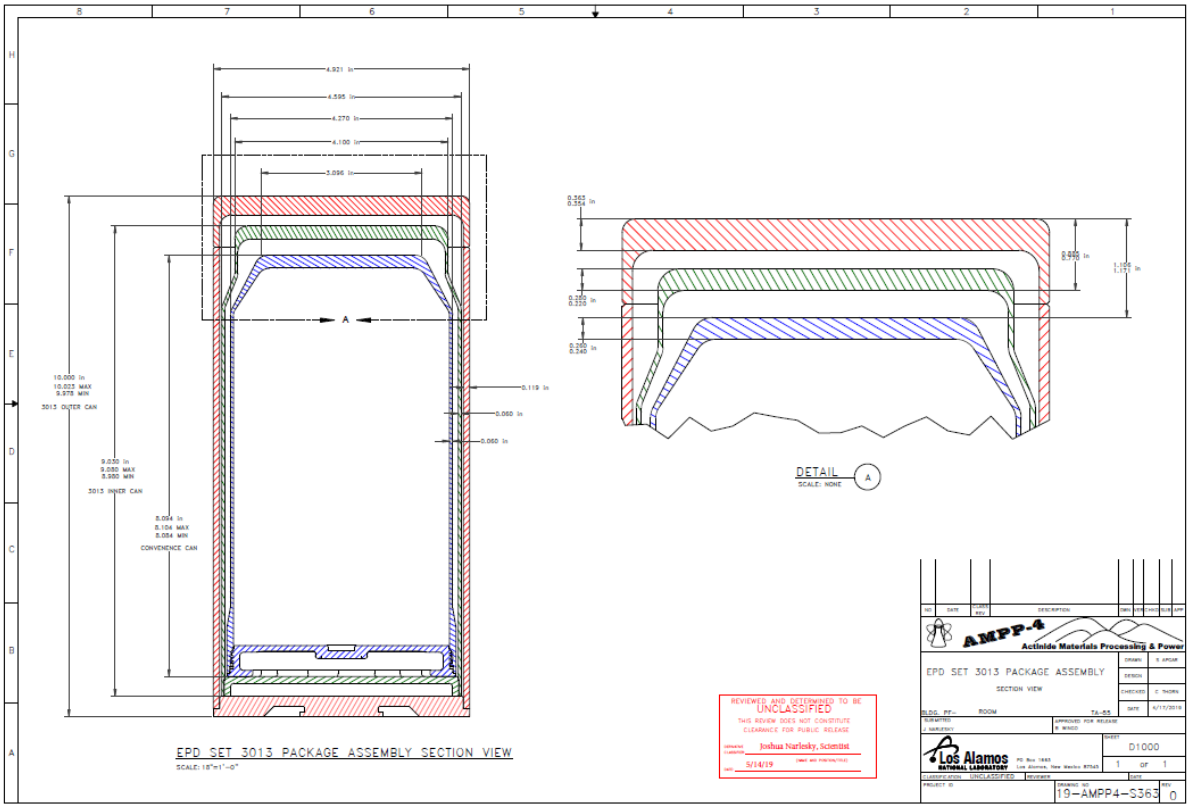

Figure 2-2. Cross-sectional drawing of the EPD assembly version (spacer inside convenience can is not shown in image).

2.1.2. Payloads

All container configurations were prepared and loaded by LANL. Within each container version, there is a variation of the composition of the payload as defined in *Recommended 3013 Loadings and Configurations for Fire Testing* and *Calculation of fill and filler masses and volumes for 3013 fire test* [7] [8]. Aluminum oxide (Al_2O_3), water (H_2O), Salts (NaCl, $CaCl_2$, KCl), stainless steel spacers, and a free volume of gas (He/air) comprise the different payloads. Gas compositions specific to each vessel prior to testing are documented in the figures of Section 7.1 in the Appendix (see first column). The payload was designed so that the free gas volume in each test vessel bounds the minimum free gas volume of the containers in inventory. The free gas volume was fixed for all the tests; the other payload parameters were varied in order to help determine what would create bounding conditions.

The aluminum oxide in the payload was used as a surrogate material for the actual payload of stored containers. The aluminum oxide used was a similar particle size with similar thermal characteristics as the actual payload it is intended to resemble. The presence of water was anticipated to affect the pressurization during thermal testing. Based on existing and expected future moisture contents for payloads in 3013 containers, both conservative and representative quantities were added to the payload in this test series. The water content bounds the maximum water content of the stored inventory plus a 20% margin [5]. Although it does not bound the amount of water theoretically allowed by the 3013 Standard, it is now highly unlikely that higher water content could be generated since the 3013 Standard has been modified to restrict the humidity allowed in packaging

gloveboxes[1]. Therefore, for the water content, either of three quantities were combined with the payload: 18 grams, 12 grams, or 6 grams of moisture. Since chloride salts are present in many of the 3013 containers, salts were added to some of the test containers to investigate the effects of high-temperature corrosion, and thus to determine whether the presence of salts affect the response and performance of a 3013 container in a fire scenario. The salts used were in mass proportions of 48% sodium chloride, 48% potassium chloride, and 4% calcium chloride. For the tests described in this paper, either of three salt masses were added to the payload: 928.5 grams, 463.8 grams, or no salt. Helium leak tests for each of the 3013 inner and outer test containers were performed by LANL immediately after container preparation to ensure an acceptance criterion of 5×10^{-8} std-cc/s was met [5].

2.1.3. Modifications to Test Units

To measure the pressure response of the 3013 containers, the containers were modified and fitted with a pressure tap and manifold system on the bottom-end of the outer 3013 containers, as shown in Figure 2-3. The modification was performed at the Savannah River Site (SRS) under an NQA-1 program [9]. In both the ARIES and the EPD set, the pressure tap is a hole drilled though the outer and inner containers; the innermost convenience can was not punctured. The innermost can however, is considered vented so that pressurized gas can escape. A stainless-steel tube is welded to the tap on the outermost container and connects to the multiport stainless-steel block that in turn connects to the fill valve and two pressure transducer ports, forming the pressure manifold as shown in Figure 2-3. The manifold system allows installation of two pressure transducers on the corresponding ports to: (1) control the initial vessel pressure prior to heating and, (2) monitor the pressure buildup during heating. (See labeled diagram of manifold in Figure 7-5 of the Appendix). The third port on the manifold was connected to the fill valve that allowed adjustment of the pre-test internal pressure with added/removed helium. In case test day temperatures differed from the vessel preparation temperatures, this latter capability allowed adjustments that would guarantee that every test would initiate with ~8.1 psig inside the container. Helium leak tests were performed at SRNL after installing the pressure manifold but prior to shipping to SNL in order to ensure leak tightness [10].

[1] These moisture loadings are considered to bound current and expected 3013 container inventories and would, in a fully loaded Pu-bearing 3013, represent 0.36 wt. %, 0.24 wt.%, and 0.12 wt.'% moisture content. DOE-STD-3013-2018 permits a moisture content of up to 0.5wt%.

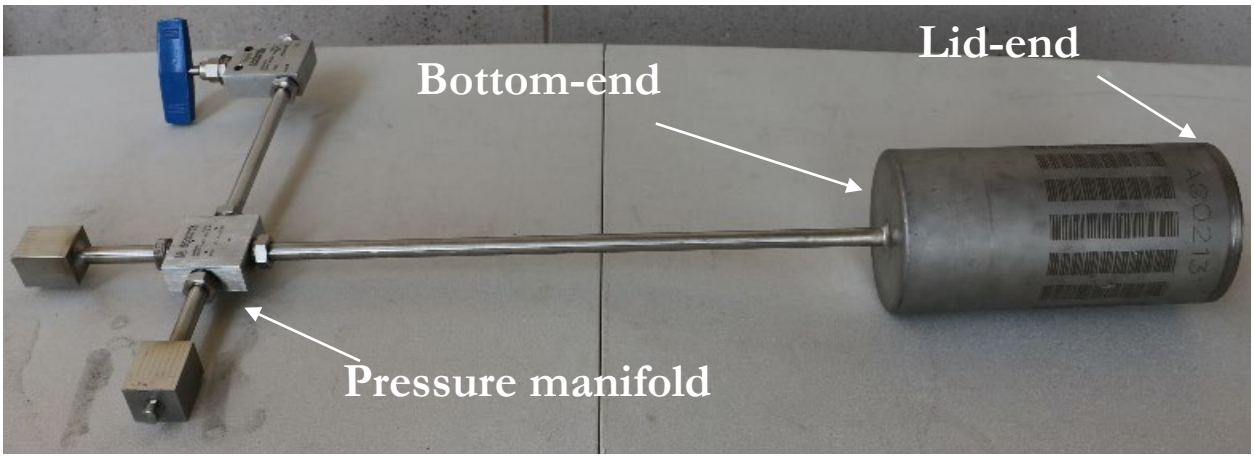

Figure 2-3. Typical tested 3013 container with welded pressure tap on bottom-end.

2.2. Instrumentation and Data Acquisition

As part of the characterization objectives, key pressures and temperatures were to be recorded during the tests. Sampling rates of 1 hertz and 1000 hertz were used for the thermal and mechanical measurements, respectively. All data were acquired to meet NQA-1 standards with SNL's Mobile Instrumentation Data Acquisition System (MIDAS). On two occasions (once with the thermal data, and once with the mechanical data), however, the data acquired with MIDAS was compromised and it was substituted with data acquired on the test facility data acquisition system.

2.2.1. MIDAS

MIDAS is a combination of commercial grade electronic equipment configured as a system to collect, store, and process data from resistive and voltage type measurement devices. MIDAS implements a contemporary data acquisition design utilizing equipment technologies available from the late 1980's to present.

MIDAS is comprised of up to ten racks of electronic equipment housed in a 44-foot trailer. The trailer, along with a portable diesel powered generator, provides a self-contained mobile instrumentation data acquisition and processing facility. Structural and thermal data are the two major types of information collected by MIDAS. The structural data collection system is capable of acquiring up to 168 channels of time domain data from multiple types of piezoresistive and voltage-based measurement devices. These measurement devices can include accelerometers, strain gages, strain gage bolts, load cells, pressure gages, and linear variable differential transformers (LVDTs). Generally, cables from these measurement devices are connected to MIDAS using two differential input interface panels, one located approximately midway along the street side of the trailer and the second located in Rack 8. In conjunction with the differential inputs, MIDAS has the capability to monitor and record 72 single ended input devices from another interface panel located in the trailer. The structural data collection system was designed to have a flat frequency response that extends to 100khz $\pm$ 0.5 dB, thereby, assuring linear recording of data up to that frequency.

The thermal data collection system is capable of acquiring and processing up to 80 channels of Type K and 20 channels of Type J thermocouple data. Thermal data can be collected and displayed in conjunction with structural data providing a unique real time capability of monitoring the thermal response of a package under test in conjunction with structural response data.

The structural and thermal data collection systems are controlled by a central system processor. The central system processor consists of a Dell Workstation Personnel Computer (PC). This computer serves as the primary data acquisition and instrument control processor and is the primary computer used by the MIDAS Operation and System Personnel to acquire structural and thermal data. A second PC based computer system (Dell Workstation) is configured to run Microsoft products. This Dell Workstation serves as the primary data analysis system, allowing the MIDAS Operation and System Personnel access to all raw data stored within MIDAS via network file system (NFS) protocols. The MIDAS computer systems are capable of performing electronic equipment control, data acquisition, and post processing of previously acquired data at the same time. Specific details on the electronic equipment used in MIDAS can be found in the MIDAS System Description (MIDAS-SD).

MIDAS position and time base information are provided by a Global Positioning System (GPS) time code receiver/translator/time code generator. This GPS receiver, along with its built in time capture capability provides test event time information with sufficient resolution to establish accurate time correlation information for structural, thermal and photometric response data. This capability was key in the test series described in this report

MIDAS it is maintained through an ongoing process that applies the applicable 18 criteria of Title 10 Code of Federal Regulations Part 71 (10CFR71, Packaging and Transportation of Radioactive Material), plus criteria 19, which is Software Quality Assurance [11].

2.2.2. Mechanical Instrumentation

A Gefran KN Series 5000 psi high temperature pressure transducer (Gefran KN2-6-M-P01M-1-5-E-I-000) was connected to MIDAS and used to measure the pressure response inside the outer 3013 container with NQA-1 quality [12]. A Gefran KN Series 1000 psi high temperature pressure transducer was attached to the second port on the pressure manifold. Both transducers had an uncertainty of ± 0.5% of the full-scale range. Inspection and installation steps for the 1000 psi pressure transducer followed the same Quality Plan as the 5000 psi transducer. However, a data acquisition system with a hardware and software Quality Plan was not used for the 1000 psi transducer, although all hardware was calibrated. However, the reading from the 5000 psi transducer was lost in one test, and the reading from the 1000 psi transducer was used as a substitute. Further details on this substitution are provided in Section 4. For both transducer types, the minimum calibrated pressure (by the manufacturer and SNL) was 100 psi, so readings below this pressure should be interpreted with care.

2.2.3. Thermal Instrumentation

Type-K thermocouples (TCs) were used to monitor surface temperatures for the outer 3013 container and shroud because of their range and accuracy (range of 0°C to 1300°C with an accuracy of ± 2.2°C or 0.75% of measurement in °C, whichever is greater). To denote TC locations, angular positions were used and were referenced in 0relation to the contact point of the vessel on the support blocks. The contact point marked the zero degrees angular position, and the remaining positions were referenced counterclockwise relative to the contact point when looking at the vessel from the lid-end. This reference point and positive angular direction for TC locations are illustrated in see Figure 2-4. A combined total of 14 TC locations were chosen to monitor temperature along the vessel and shroud using the MIDAS data acquisition system; 11 TCs on the vessel, and three on the shroud. Table 2-1 maps the labels used to their corresponding locations, where the "M" prefix on the numbering indicates that the TC was connected to MIDAS. Figure 7-3 and Figure 7-4 in the Appendix respectively provide isometric views of the vessel and shroud with illustrated TC locations for all TCs tabulated in Table 2-1. These figures also identify thermocouples that are not shown in Table 2-1. These remaining TCs, which can be identified by the missing "M" in their labels, correspond to TCs that were not connected to MIDAS and therefore were not connected to a data acquisition system with a verified hardware and software quality plan. Table 2-2 tabulates this second set of TCs and maps them to their respective locations. While this second set of TCs was not connected to MIDAS, all protocols followed to install and inspect functionality for these TCs were the same as those that were connected to MIDAS. These thermocouples were installed by SNL to monitor vessel and shroud response from SNL's Thermal Test Complex (TTC) control room during a test. When the readings from the MIDAS TCs were compromised in one occasion, the thermocouples from the TTC control room had to be used as a substitute. Further details on this substitution are provided in Section 4. Lastly, to ensure consistent temperatures for the pressure manifold, a heater rope was used to ensure temperatures in the manifold area were near 200°C. TCs were used to monitor and ensure this specification was met, but these temperatures were not recorded with MIDAS and are therefore not presented in this report. Nonetheless, it should be noted that no anomalies were registered for the manifold temperatures.

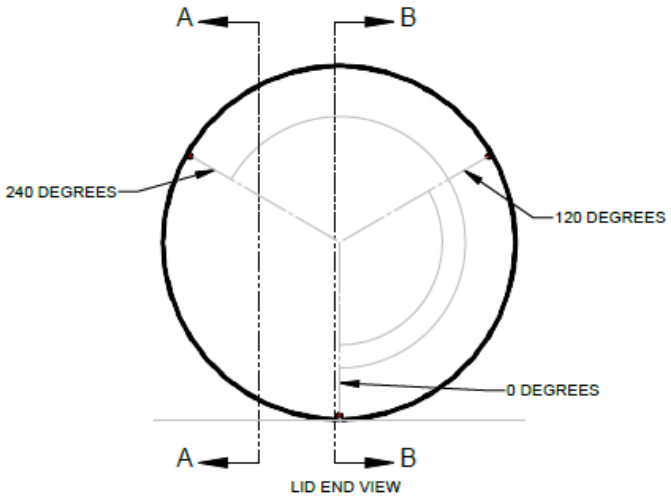

Figure 2-4. Angular reference points, looking into the lid-end of shroud. The 0 degrees reference point is where the vessel makes contact with the saddle.

Table 2-1. NQA-1 Thermocouples

TC Name	TC Location	Component
TC M01	Lid Center	Vessel
TC M02	Lid Offset	
TC M03	Lid-end, 240°	
TC M04	Bottom-end, 240°	
TC M05	Lid-end, 0°	
TC M06	Middle, 0°	
TC M07	Bottom-end, 0°	
TC M08	Lid-end, 90°	
TC M09	Bottom-end, 90°	
TC M10	Bottom lower offset	
TC M11	Bottom outer offset	
TC M12	Middle, 0°	Shroud
TC M13	Middle, 120°	
TC M14	Middle, 240°	

Table 2-2. Non-NQA-1 Thermocouples.

TC Name	TC Location	Component
TC 01	Middle, 240°	Vessel
TC 04	Lid-end, 0°	Shroud
TC 06	Lid-end, 120°	
TC 07	Bottom-end, 120°	
TC 08	Lid-end, 240°	
TC 10	Middle, 0°	Vessel
TC 11	Lid-end, 90°	

2.3. Heater Configurations and Test Setups

The heat source used to generate the thermal test environment for this test series was a cylindrical radiant heat setup. Figure 2-5 illustrates the configuration used for all tests in this series, where all key components are labeled. The radiant heat setups consisted of a ceramic heater body that houses silicon carbide heater rods. The specific heater designs were custom-made, and each heater consisted of 21 heater rods with a one-inch outer diameter and a cold resistance of ~2 ohms. Heater rod spacing was per the manufacturer specs. To provide uniform heating on the test specimen, an Inconel shroud was placed in between the heater rods and test containers. The heater rods and shroud were therefore concentric with the test specimen. This type of configuration allowed the heater rods to heat the shroud, and the shroud in turn heated the container. TCs welded on the shroud were used to monitor source temperatures to ensure the intended heating profiles met the heating specifications (discussed in next sub-section). The heater configuration was designed with five main design constraints:

1. Prior tests, conducted on the primary containment vessel that holds the 3013 containers, identified that a horizontal orientation of the vessel leads to higher pressurization when exposed to a fire [4]. Thus, to capture a conservative scenario, the test specimen in this series was to be tested in a horizontal orientation.
2. In case the test specimen swelled during heating and consequently rolled to the side, the heater design needed to allow movement without locking (and therefore straining) the pressure tap/manifold.
3. Space for the pressure tap and thermocouples to exit the heater body had to be incorporated in a way that did not impact the imposed flux on the test specimen.
4. The shroud could not obstruct expansion of the test vessel in case its pressurization induced swelling.
5. The test specimen had to be concentrically supported inside the shroud in a way that allowed it to receive a uniform heat flux to the greatest extent possible.

To address constraints (1) through (3), the heater was designed to sustain the test subject in a horizontal orientation with slots in the heater endcap insulation to allow routing for the pressure tap and TCs. Once installation of the vessel inside the heater assembly occurred, the slots were covered with flexible blanket insulation to minimize radiative and convective heat losses to the ambient but still permit movement of the pressure manifold. On the exterior of the heater, a support structure was designed to hold the manifold in place while simultaneously allowing movement in case of vessel swelling/rolling. Figure 2-6 illustrates these exterior design features in the setup, which shows how the manifold support was designed to allow movement and ensure that the pressure tap would not strain and result in an inadvertent failure point. By the same token, the diameter of the shroud was designed to be four inches larger than the outer diameter of the outer 3013 container in order to address constraint (4) and prevent obstruction of the vessel expansion by the shroud.

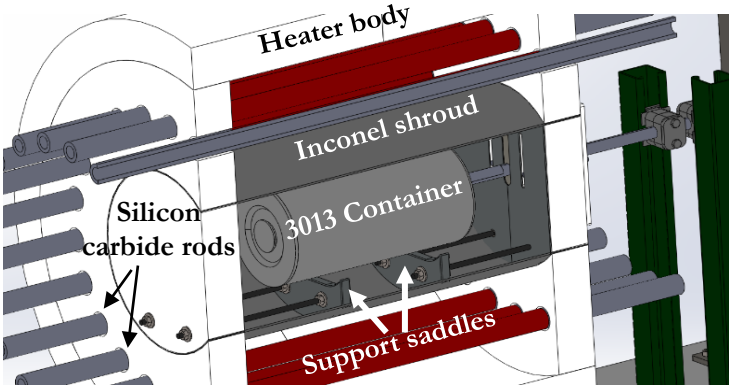

Figure 2-5. Heater configuration.

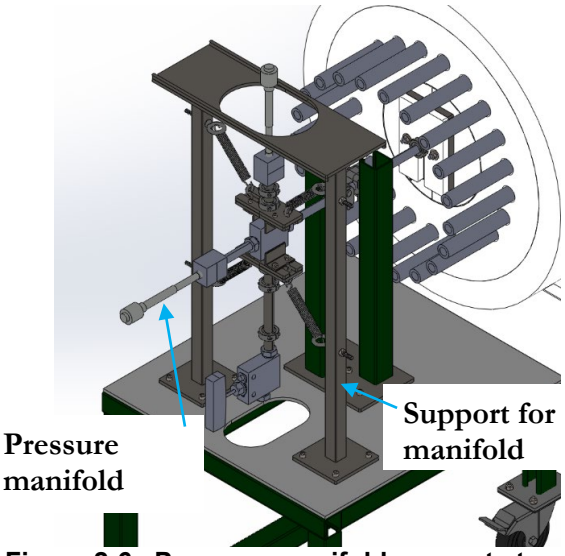

Figure 2-6. Pressure manifold support structure.

To address constraint (5), a thermal finite element analysis (FEA) was performed to analyze various design concepts for supporting the 3013 containers inside the heater. Various support systems were considered prior to modeling, but the designs with the support saddles (as shown in Figure 2-5) were the focus of the FEA work. Primarily, the model was created to ensure that any cold spots generated [on the contact points of the vessel with the support saddles] during the transient phase would not be so large as to have an unintentional adverse effect on the outcome of a test. The model was simulated using ANSYS 2019 R2, and it was simplified to only model the shroud, vessel, aluminum oxide payload, heater end caps, and support blocks. The vessel design was further simplified so that the masses of the three containers (outer, inner, and convenience can) and spacer were merged into one volume to avoid solution divergence resulting from thin materials with multiple contact resistances. Figure 2-7 illustrates the simplified FEA model. The simulated heat-up was based on the faster heating curve (ASTM-E1529, discussed in detail in next section) in order to capture a more conservative scenario. After performing a suite of steady and transient simulations, it became obvious that the period with the larger thermal gradients (located near the contact points between the vessel and support saddles) would be in the transient phase during the first 10 minutes of heating. Through some iterations on the radiative parameters, it also became apparent that

increasing the reflectivity of the heater endcaps and support blocks would benefit the transient phase. Ultimately, the chosen configuration was with two support saddles/blocks positioned two inches from the ends of the test vessel. Figure 2-8 shows contour plots along the bottom of the container for 10 minutes of simulation time when using an ASTM-E1529 heating profile. The larger gradients at the contact points (approximately two-inches from the ends) are observed near 5-6 minutes, after which thermal diffusion relaxes these gradients. This analysis supported the decision for the chosen configuration.

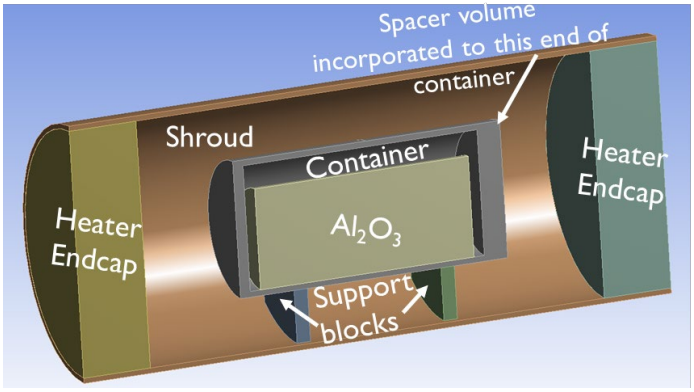

Figure 2-7. Cross-section of simplified model used for FEA thermal analysis

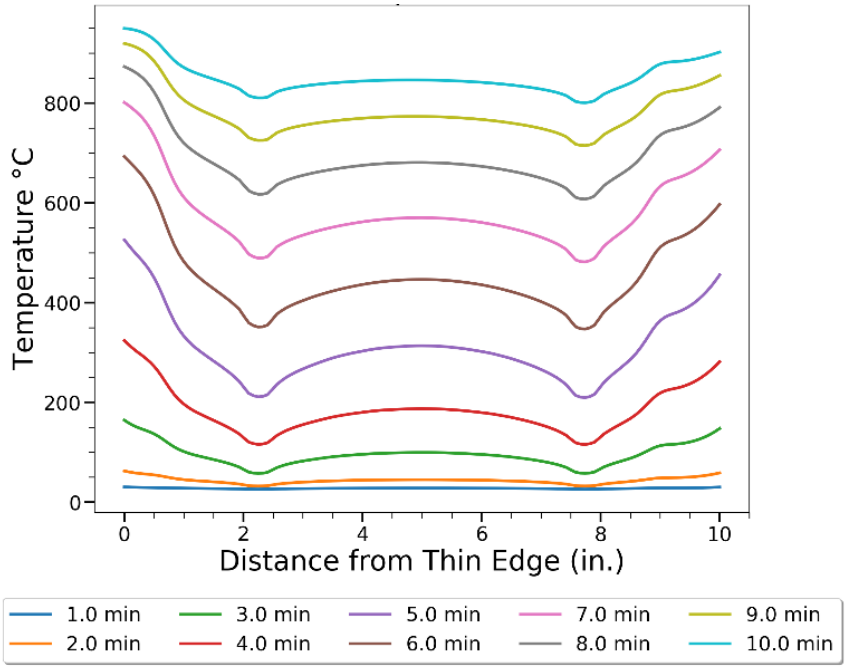

Figure 2-8. Transient temperature profiles along bottom of 3013 container as calculated from a thermal FEA model for the first 10 minutes of heat-up.

2.4. Heating Profiles

To create the fire environment for the test vessels, the radiant heat setups were operated with a control system to match desired heating profiles. As mentioned in the Introduction, two heating profiles used in this test campaign were chosen as representative and conservative test profiles given the storage sites where 3013 containers reside; one with a more aggressive heating ramp than the other. Table 2-3 and Figure 2-9 highlight the variations between the two profiles. For the slower heating ramp, a slight modification of the heating curve prescribed by ASTM-E119 (*Standard Test Methods for Fire Tests of Building Construction and Materials*) was chosen [13]. For this milder case, the heat source was set to follow the ASTM-E119 heating curve until reaching 1500°F but then it was to remain at that temperature for the remainder of the test. The modification was chosen to represent a bounding impingement temperature from an ordinary combustible exposure fire. Due to this modification, that heating profile will be referred to as the ASTM-E119m profile for the remainder of this report. Key markers that denote how the profile should ramp up are tabulated in Table 2-3. Figure 2-9 helps visualize these markers, where the heat source is required to reach 1000°F (538°C) in the first 5 minutes, 1300°F (704°C) by 10 minutes, and 1500°F (816°C) by 30 minutes but persist there for the remainder of a test.

Table 2-3. Time markers for heat source required by ASTM heating profiles

E119m Times	E119 Temps	E119m Temps	E1529 Temps	E1529 Fluxes
3 min.	Not specified	Not specified	815°C	Not specified
5 min.	1000°F / 538°C	1000°F / 538°C	1010°C	158 kW/m^2 ± 8 kW/m^2
10 min.	1300°F / 704°C	1300°F / 704°C	Between 1010°C and 1180°C	158 kW/m^2 ± 8 kW/m^2
30 min.	1550°F / 843°C	1500°F / 816°C	Between 1010°C and 1180°C	158 kW/m^2 ± 8 kW/m^2
1 hr.	1700°F / 927°C	1500°F / 816°C	Between 1010°C and 1180°C	158 kW/m^2 ± 8 kW/m^2
2 hr.	1850°F / 1010°C	1500°F / 816°C	Between 1010°C and 1180°C	158 kW/m^2 ± 8 kW/m^2
4 hr.	2000°F / 1093°C	1500°F / 816°C	Between 1010°C and 1180°C	158 kW/m^2 ± 8 kW/m^2

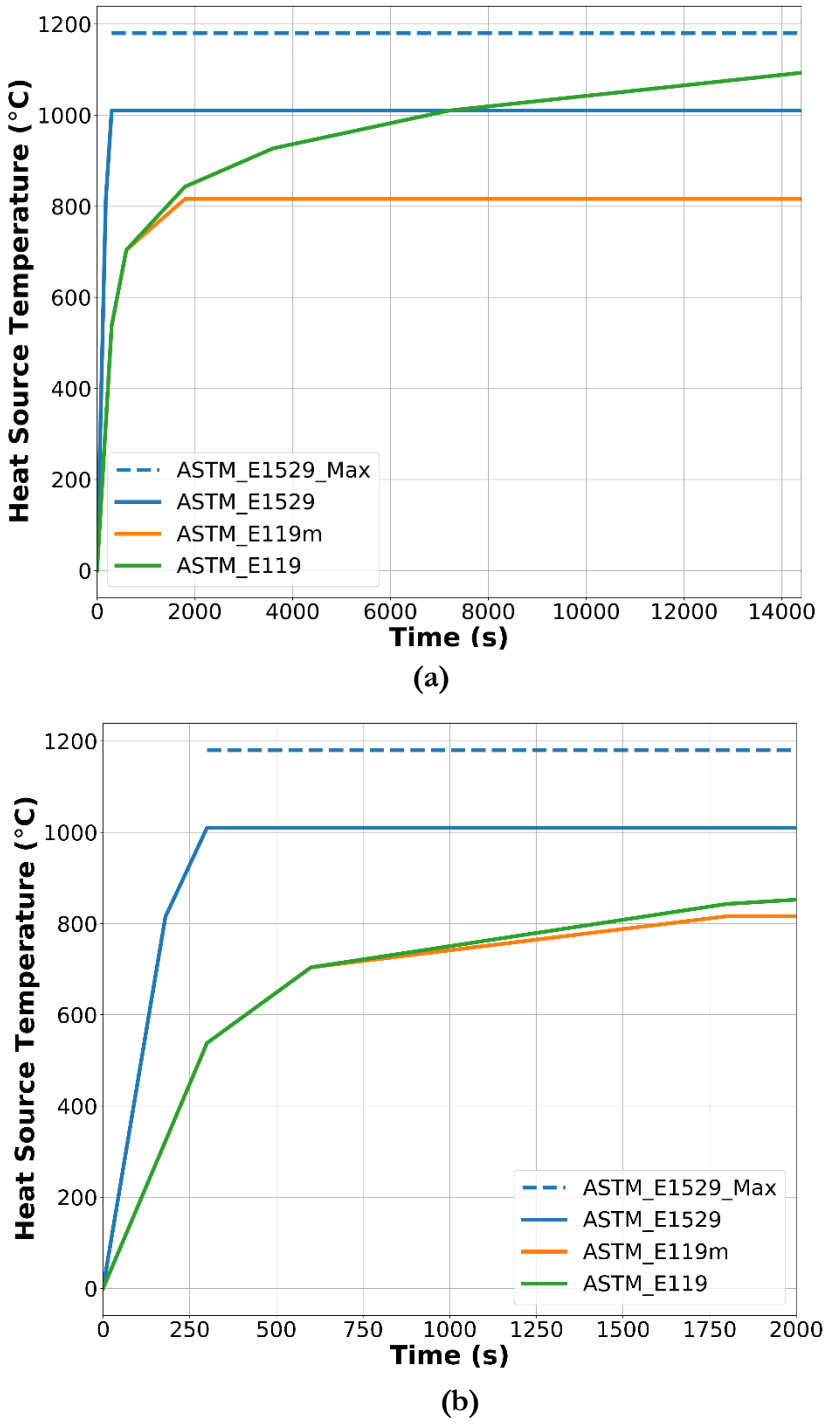

Figure 2-9. ASTM Heating Profiles. (a) Shows 4 hours of test time, (b) zooms in on 2000 seconds.

For the more aggressive thermal insult, the heating curve prescribed by ASTM-E1529 (*Standard Test Methods for Determining Effects of Large Hydrocarbon Pool Fires on Structural Members and Assemblies*) was chosen because it represents the bounding conditions for a 3013 container engulfed in a combustible liquid spill fire scenario [14]. With the ASTM-E1529, the heat source is required to reach 815°C by three minutes, 1010°C by 5 minutes, and shall remain between 1010°C and 1180°C

for the remainder of the test. The requirements on ASTM-E1529 also specify that a flux of 158 $kW/m^2 \pm 8\ kW/m^2$ shall be imposed on the test specimen within the first 5 minutes of test exposure and shall sustain there for the remainder of the test.

The heat flux requirements of ASTM-E1529 required knowledge of the imposed heat flux on the test vessel for a given shroud temperature. Given the dimensions of the test subject, heat flux sensors would be difficult to incorporate into a radiant heat setup without affecting the heat flux imposed on vessels. A calorimeter was designed to correlate the imposed heat flux on the test specimen with the heat source temperature. To maintain representation, the geometry, materials, payload, and mass of the calorimeter were matched to that of the 3013 containers. Figure 2-10 illustrates sample isometric views of the calorimeter. Schmidt-Boelter heat flux sensors were placed on the walls of the calorimeter to correlate incident flux on the vessel with measured shroud temperatures. A payload was used to match that of the tested vessels, and a cross-section of the payload is depicted in Figure 2-10a as the shaded light-brown material filling the vessel. Figure 2-10b suppresses the payload to show how a second configuration was implemented with an additional sensor on the lid-end of the calorimeter to provide a reading for the heat flux received by the test unit at the ends. Mock tests were run on an un-instrumented calorimeter to define the transient heater power input required to produce the ASTM-E1529 temperature profile. Once the heater power was defined to produce the ASTM-E1529 temperature profile, an instrumented calorimeter was subsequently run. These latter calorimetry measurements assured that the heat flux criteria of ASTM-E1529 were met. Thorough details of the calorimeter are provided in *Correlating Incident Heat Flux and Source Temperature to Meet ASTM-E1529 Requirements for RAM Packaging Components Thermal Testing* [15].

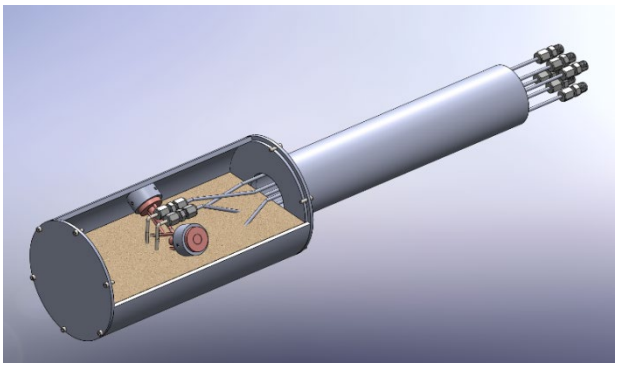

(a)

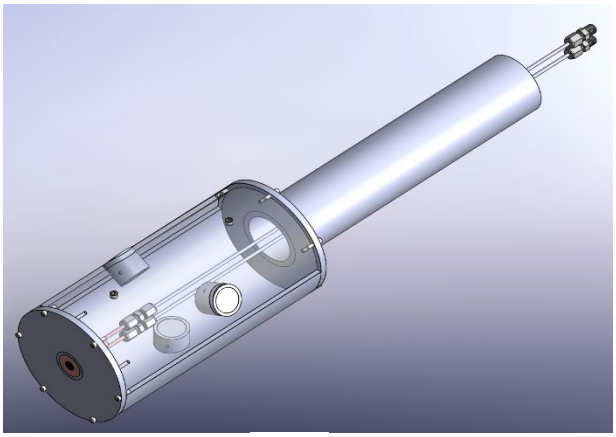

(b)

Figure 2-10. Calorimeter schematic.

Figure 2-11. Calorimeter schematic. (a) Shows how payload was used in calorimeter tests, and (b) suppresses the payload to show how heat flux sensors were oriented

2.5. Gas Sampling and Leak Tests

Gas sampling was completed three times for each container: (1) as-received after the pressure transducers were installed, (2) after the pressure manifold leak testing was complete, and (3) after thermal testing was complete. Retrieving the samples was a part of the test plan for the as-received unit following the pressure transducer installation and after the pressure manifold leak testing was complete (items (1) and (2) above). The third gas sample was conducted in the same manner as (1) and (2), and while it was not specified in the test plan for this test campaign, it is also documented in the Quality Assurance (QA) package delivered to SRNS. Gas analysis of all three samples for each container was conducted using an "Internal Vapor Analyzer Time of Flight Mass Spectrometer" (IVA-TOF) Oneida Research Systems Model 210s, high resolution gas analyzer. Results from this gas sampling are briefly presented in Section 4.

Leak testing at SNL was completed two times for each container: (1) as received after the pressure transducers were installed and (2) after the thermal test was completed to check for any breach

points[2] [10]. Leak testing was conducted using a Helium Leak Detector manufactured by Pfeiffer Vacuum Adixen ASM 390. The first leak test at SNL was conducted per the test plan on the pressure manifold to ensure leak tightness of the setup with pressure transducers installed. The second leak test at SNL was noted in the QA documentation and was conducted on the container to find leaks post-thermal testing, and it was performed by a third party (Scientific Vacuum). Since the post-test checks did not target leaks on the fittings of the vessel configurations but were rather performed with the intention of finding a breach point, they are referred to as breach tests. The process for the post-thermal test breach testing consisted of three primary steps. The first step was to evacuate the container down to a background signal of 1E-7 atm-cc/sec He and observe the behavior of the helium signal. Then a helium overspray test was performed on the container. If there was no spike in signal, the test was complete, and the vessel was considered to not have a breach point. If there was a spike in the signal or the background would not get to 1E-7 atm-cc/sec He, an overspray test would be performed until a positive location for the breach was identified. The location would be marked, double checked, the location was marked for documentation, and then the test would be complete. These results are briefly presented Section 4.

[2] Note that prior to the leak testing at SNL, leak testing was performed for the first time at SRNL after installation of the manifold assembly

3. TEST MATRIX

In Section 9 of the test plan (*PCV/SCV/3013 Thermal Test Program Phase 3 Test Plan Rev. 0*), the test matrix for the campaign was outlined by a given "Test #". Due to unexpected outcomes with the first test, the remaining tests in this campaign were executed in an order that resulted in those "Test #'s" being out of sequence. Therefore, for readability purposes, this report discusses the tests using a sequential numbering system, and each test is referred to by "Sequence #" instead of "Test #" to indicate that these assigned numbers are different. The "Test #" format is not used in the remainder of this report, but Table 3-1 is documented here to map "Sequence #'s" from this report to the "Test #'s" described in the test plan. In addition, the unique container identification number (CID-#) for the vessel in each test is also documented in Table 3-1 as those numbers remained fixed from the moment the vessels were prepared for testing. Table 3-1 outlines the nomenclature changes between the test plan and this report, and it should be referenced by any reader that refers back to the test plan.

Table 3-1. Crosswalk between Sequence #'s used in this report and Test #'s used in Test Plan.

Sequence #	CID #	Test # (from Test Plan)
1	3	1
2	2	3
3	6	5
4	10	2
5	12	8
6	4	9
7	5	4
8	8	10
9	11	7
10	9	6

Table 3-2 below outlines the complete test matrix for these studies. As previously stated, two versions of the 3013 outer container were of interest for the test campaign discussed here. Five tests were performed on the EPD version of the 3013 container, and another five were performed on the Flowform version of the 3013 container. As stated in the Introduction, the tests discussed in this report focused on testing conservative scenarios, where the alumina payload contained various combinations of salt and moisture (H_2O). As mentioned in Section 2.2, capturing vessel response for two different heating profiles were also of interest in this test series. The first and last test were exposed to the ASTM-E119m heating profile, while the remainder of the tests were exposed to the ASTM-E1529 heating profile. Aluminum oxide powder was used as a surrogate for the actual payload and the loadings ranged from ~642 g to ~1958 g. Moisture content in the payload varied between 6 g and 18 g, and salt was added to two out of the five vessels for each container version in quantities of either 928.5 g or 463.8 g. For the test execution, an initial heat-up period of approximately 15 minutes was incorporated at the beginning of the tests to allow the shrouds to reach 100°C. When the shroud reached 100°C, the beginning of a test was marked, and the prescribed heating profile followed. Heating to the vessels was maintained for four hours or until an

obvious breach was observed in the test vessel. Any stoppages resulting from a vessel breach were defined by a sudden pressure drop in the vessel, and termination of power to the heaters only occurred if approved by SRNS. The next section discusses the outcomes and corresponding implications of the tests described in Table 3-2.

Table 3-2. Test Matrix.

Sequence #	3013 Outer Container Version	Al_2O_3 content (grams)	H_2O content (grams)*	Salt content (grams)	Initial Pressure (psig)	Lab Pressure (psig)	ASTM Heat Profile
1	EPD	1572.6	18	0	8.128	N/A	E119m
2	EPD	1572.6	12	0	8.102	N/A	E1529
3	EPD	642.1	12	928.5	8.100	N/A	E1529
4	Flowform	1958.5	12	0	8.243	N/A	E1529
5	Flowform	734.1	12	928.5	8.135	N/A	E1529
6	EPD	1572.6	6	0	7.946 **	8.100	E1529
7	EPD	1107.0	6	463.8	7.877 **	8.181	E1529
8	Flowform	1958.5	6	0	7.908 **	8.100	E1529
9	Flowform	1493.2	6	463.8	8.064 **	8.100	E1529
10	Flowform	1958.5	6	0	7.982 **	8.100	E119m

* *Represents maximum moisture content in SRS inventory. DOE-STD-3013 permits 0.5 wt.% (25 g) moisture.*

** *Represents "Initial Pressure" that was calculated using ideal gas law after measuring pressure in lab at 21.1°C.*

4. RESULTS & DISCUSSION

As previously mentioned in this report, the tests are referred to by their Sequence #, which is the sequential order in which tests were carried out. Nonetheless, the Sequence #'s are always mapped to the corresponding CID #, which is key to identifying the characteristics of each container. Table 4-1 below provides an overview of the results for the test series discussed here with the CID #'s mapped to the Sequence #'s. Peak pressures observed by each vessel are recorded in this table along with their corresponding times as referenced from the point at which the 15-minute heat up started. In general, the pressures observed were lower than those calculated using the ideal gas law and steam tables. One phenomenon reducing the pressure is that the container bulges so the internal volume increases. The volume increase was not measured, but it appears to have a relatively small effect on the pressure. The other phenomenon that has a larger effect on pressure is that the steam reacts with the hot container wall. This reaction forms metal oxides, a small amount of metal hydrides and hydroxides, and hydrogen gas. A portion of the remaining hydrogen gas then diffuses and permeates through the stainless-steel wall at high temperature. The diffusion and permeation rates increase significantly as the temperature increases [16]. This can be observed as a slow reduction in pressure after the maximum pressure is reached. Another observation is that the pressures are higher for containers with salt. In these containers, some of the water reacts with the calcium chloride salt and for each mole of water reacted, one mole of calcium oxide and two moles of HCl gas is formed.

Results from breach checks performed after test exposure are also included for each vessel. Out of the 10 tests, six were found to have some form of breach. For those tests exposed to the ASTM-E119m curve, no breach points were found in either test. For those tests exposed to the ASTM-E1529 curve, only those vessels that experienced pressures over 200 ± 25 psig were found to have been breached. All vessels with added salts experienced a breach, independent of the outer container version. For those vessels without added salts, only those tests on the Flowform version of the outer container experienced a breach. The EPD containers with no added salts were not breached, independent of the amount of moisture in the vessel. Furthermore, for any given set of conditions, the Flowform configurations experienced higher peak pressures under comparable heating and payload conditions. The reason for this is not fully understood, but the inner containers and convenience cans in the Flowform configuration have a significantly different design from the ones in the EPD configuration. It is possible that these differences affect the thermal gradients inside the containers during the tests and the rate at which water can escape the convenience container to react with the hotter outer container wall.

All of the breach points observed after the tests were completed were very small openings that required helium leak testing to locate. In no case was a large opening observed as was seen in the previous room temperature hydro tests performed for outer container qualification. To assist in material release calculations, an attempt was made to quantify the amount of surrogate material lost from containers that failed. The scale used to measure the container and associated instrumentation before and after the test was an *Arlyn Scales Model SAW-HL-RS-232-USB* scale with a range of 0-90 kg and an uncertainty of 1 gram. The high temperatures imposed on the vessels, especially from the ASTM-E1529 curve, caused the outer surface of the containers to oxidize and flakes spalled off. This "debris" was collected from the shroud, weighed, and converted to the constituent metal mass. It is concluded that if there was any surrogate powder expelled from the failed containers, the quantity was a small fraction of the mass loss listed in Table 4-1. The subsections below present a comprehensive discussion for the pressure and thermal response of each vessel throughout the

duration of each test. In all tests described below, keys for thermocouple locations shown in the plot legends are as referenced in Table 2-1 and Table 2-2 in Section 2.2.

Table 4-1. Test Series Results.

Sequence #	CID #	3013 Outer container version	H_2O content (grams)*	Salt content (grams)	Peak press. (psig)*	Time @ Peak Press. (s)	Time of pressure drop when breached (s)	Breach test results	Mass loss (grams)**
1	3	EPD	18	0	169 ± 25	7272	N/A	No breach @ 2.8E-8 atm-cc/sec He	0
2	2	EPD	12	0	123 ± 25	3327	N/A	No breach @ 1.0E-7 atm-cc/sec He	36
3	6	EPD	12	928.5	284 ± 25	3116	~3470	Breach around 180º near lid weld	13
4	10	Flowform	12	0	324 ± 25	2630	~2880	Breach around 100º	48
5	12	Flowform	12	928.5	332 ± 25	2102	~2460	Breach around 200º Near Barcode	5
6	4	EPD	6	0	186 ± 25	3789	N/A	No breach @ 1.4E-8 atm-cc/sec He	38
7	5	EPD	6	463.8	229 ± 25	3430	~6000	Breach around 300º at lid weld	0
8	8	Flowform	6	0	244 ± 25	2899	~4840	Breach around 80º near axial center of unit	10
9	11	Flowform	6	463.8	253 ± 25	2251	~3970	Breach around 110º near axial center of unit	19
10	9	Flowform	6	0	262 ± 25	14884	N/A	Not breach tested***	-8

***** Due to uncertainty in transducers being **±** 25 psi, recorded pressures are rounded to nearest integer

****** Mass loss does not include metal flakes that spalled into the shroud because it was impossible to quantify what percentage came from the container outer surface and what percentage came from other components.

******* No sign of pressure loss or breach noticed during thermal test

4.1. Sequence 1: CID-3

With this first test, the goal was to evaluate the vessel with the largest amount of H_2O as it seemed to have the largest potential for heat-induced pressurization. Sequence 1 was an EPD version of the outer container with 18 g of H_2O and no salt. The heating profile used was the ASTM-E119m profile. The thermal and pressure response for Sequence 1 are captured in Figure 4-1, and the post-test conditions of the vessel are captured in Figure 4-2. Thermocouple locations are as described in Table 2-1. The ASTM-E119m heating profile can be recognized in the figure by its heating rate and by the peak temperatures observed. The initial 15-minute warm-up period up to 100°C is shown in the early portion of Figure 4-1. As expected, the vessel TCs lag behind the shroud TCs. This warm-up period along with the lag in thermal response is observed in all tests, even in tests with the ASTM-E1529 heating profile, so it is therefore only mentioned in this test sequence to avoid repetition.

This test ran for the full four hours (Figure 4-1 shows a gap in the pressure reading, and this results from the MIDAS system having a max recording time of 3 hours and 45 minutes. The logging system thus has to restart to capture the full 4 hours of test time. The logging system takes a few minutes to restart, and this results in a short period of non-recorded data. This gap is seen in all tests that last the full test time). The peak pressurization observed in the outer container was 169±25 psig, but it was not significant enough to result in an obvious breach of the vessel. The post-test helium overspray test demonstrated no breach at less than 1.0×10^{-7} scc/s He. As discussed in Section 4, this pressure was lower than anticipated based on ideal gas expansion. The peak pressure experienced by the vessel was also observed before the end of the test. Figure 4-1 shows the vessel after test exposure from four angular positions (0°, 90°, 180°, and 270° in a clockwise direction), where it can be seen that no swelling or rupture of the vessel occurred (indicating that the reduced pressure observed was more likely to be as a result of (2) above). Mass loss was not registered for this vessel either. Due to these results significantly deviating from expectations based on ideal gas expansion, it was decided that the subsequent 8 vessels would be tested using the more aggressive ASTM-E1529 heating profile.

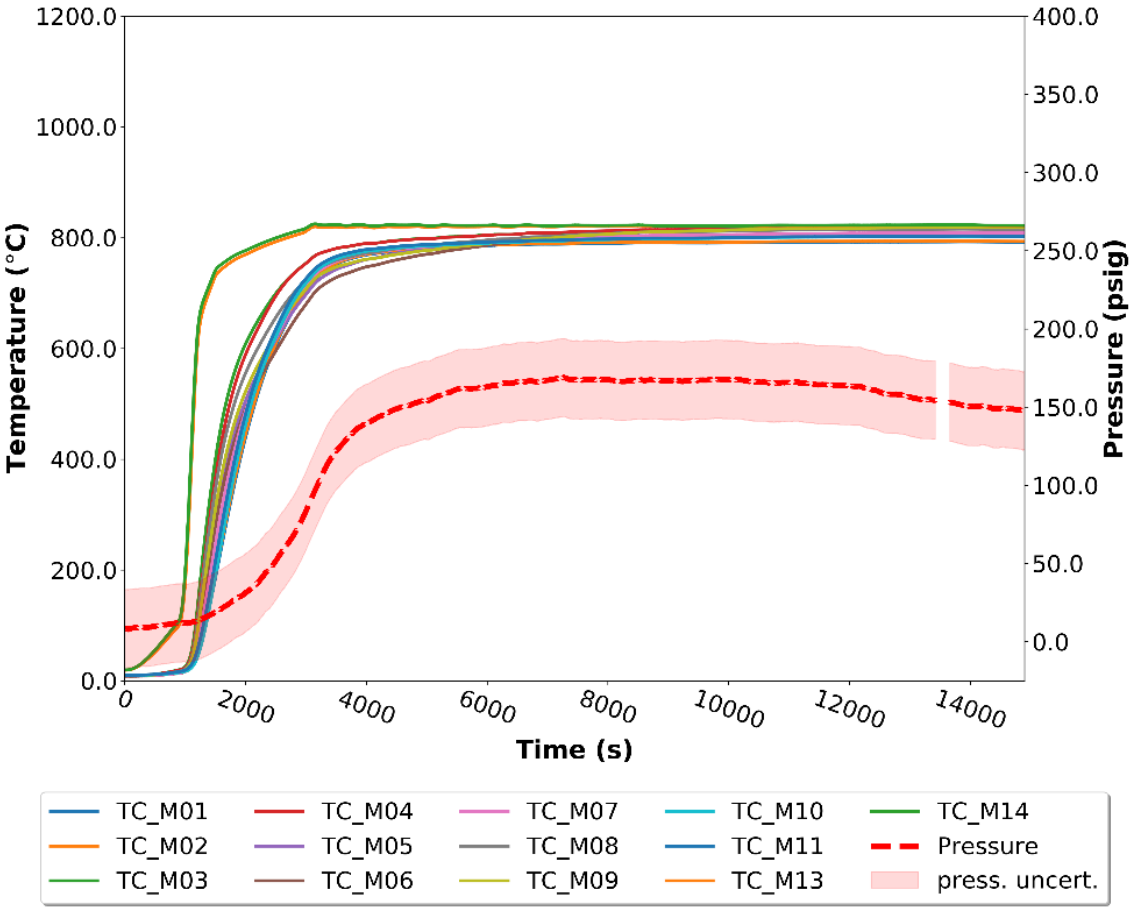

Figure 4-1. Temperature and pressure for Sequence 1.

Figure 4-2. Post-test conditions of test vessel for Sequence 1. Angle positions refer to the visible portion of the vessel (see Figure 2-4). Angular positions, in clockwise direction, starting from upper left quadrant: 0°, 90°, 180°, and 270°.

4.2. Sequence 2: CID-2

Sequence 2 tested an EPD version of the outer container with 12 g of H_2O and no salt. The heating profile used was the ASTM-E1529 profile, and this test also lasted four hours. The thermal and pressure response for Sequence 2 are captured in Figure 4-3, and the post-test conditions of the test vessel are captured in Figure 4-4.

The thermal range and temperature profiles of Figure 4-3 show how the heating profile of Sequence 2 differed from Sequence 1 and was specific to ASTM-E1529. The sharp ramp rate and higher peak temperatures unique to ASTM-E1529 can be similarly noticed in Sequences 2 through 9, and it is therefore only mentioned here to avoid repetition. While heating was faster with this profile, the peak pressure observed by this vessel was lower than Sequence 1, at 123 ± 50 psi. However, two key observations can be noticed when looking at the pressure profile for the entire test time: (1) the peak occurred almost 4,000 seconds sooner than Sequence 1, and (2) it can be seen how the pressure slowly but consistently dropped throughout the test after experiencing this peak pressure early on. This drop wasn't a sudden pressure drop to be considered a rupture, so the test persisted for the full four hours. However, the pressure did drop down to approximately 52 ± 25 psig by the end of the test. Post-test vessel inspections found the vessel to have some swelling with deformation near the lid area (see Figure 4-5). To verify whether a breach was observed by the vessel, a post-test helium leak test was performed by SNL to check for breach points, and the container demonstrated no

breach at less than 1.0 x 10^{-7} scc/s He. As discussed in Section 4, the observed decrease in pressure is likely the result of hydrogen gas, which is generated when moisture reacts with the stainless steel, permeating through the container wall at elevated temperature [16]. In addition, the vessel did experience some visible swelling that would be partially responsible for a pressure drop, but quantifying the exact volume increase as a result of the deformation was beyond the scope of these tests. Approximate measurements showed the vessel increased ~1.25 cm in length and ~.05 cm diameter at the sites of maximum deformation.

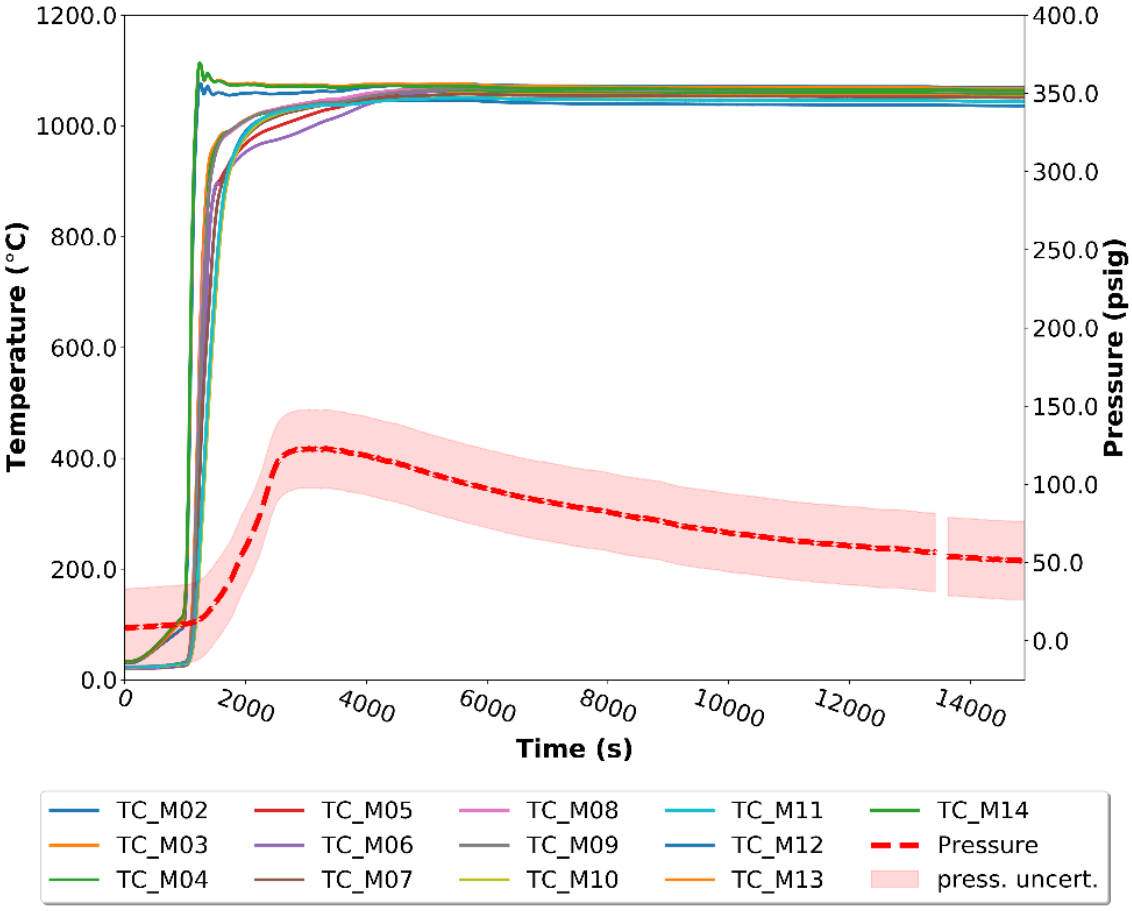

Figure 4-3. Temperature and pressure for Sequence 2.

Figure 4-4. Post-test conditions of Sequence 2. Angle positions refer to the visible portion of the vessel (see Figure 2-4). Angular positions, in clockwise direction, starting from upper left quadrant: 0°, 90°, 180°, and 270°.

Figure 4-5. Deformation around lid region of vessel in Sequence 2.

4.3. Sequence 3: CID-6

Sequence 3 tested an EPD version of the outer container with 12 g of H_2O and 928.5 g of salt. The heating profile used was the ASTM-E1529 profile. The thermal and pressure response for Sequence 3 are captured in Figure 4-6, and the post-test conditions of the vessel are captured in Figure 4-7. It should be emphasized that the thermocouples shown in Figure 4-6 are different from the previous two tests. The MIDAS thermocouples were lost early on in the test, so the thermal profiles in Figure 4-6 reflect the non-NQA-1 thermocouples recorded by SNL's TTC data acquisition system. A non-conformance report (NCR) was filed in the QA package to document this issue (NCR #5). The NCR discusses how the temperature data acquired from SNL's TTC system was comparable to (and within the uncertainty bounds of) the MIDAS data in the early part of the test (before the MIDAS thermal data was compromised), therefore making the substitution of the thermal data permissible. Furthermore, all procedures followed to ensure quality on the MIDAS acquisition systems were also followed for the TTC's thermocouples and data acquisition system.

The payload in the vessel of this third test was similar to the second test in the amount of moisture present, but it differed with the inclusion of salts. The thermal response was similar to that of Sequence 2, which was expected given the same heating profile. The pressure response, however, was significantly different. First, the peak pressure observed in this test was much larger, reaching 284 $\pm$ 25 psig near 3100 seconds. Then, just before reaching 4000 seconds, the vessel was breached as noted by the sudden drop in pressure. Considering that the primary difference between Sequence 2 and Sequence 3 was the added salt content in the payload, as discussed in Section 4, the added salt

was deduced to result in larger pressurization than for water alone. Heating in this test was allowed to continue for 6450 seconds, at which point the test was terminated. Post-test leak checks identified a breach to be near the 180° position at the lid weld on the vessel (see red mark in Figure 4-7, 180° image), and the measured mass loss for the vessel in this test was ~13 grams.

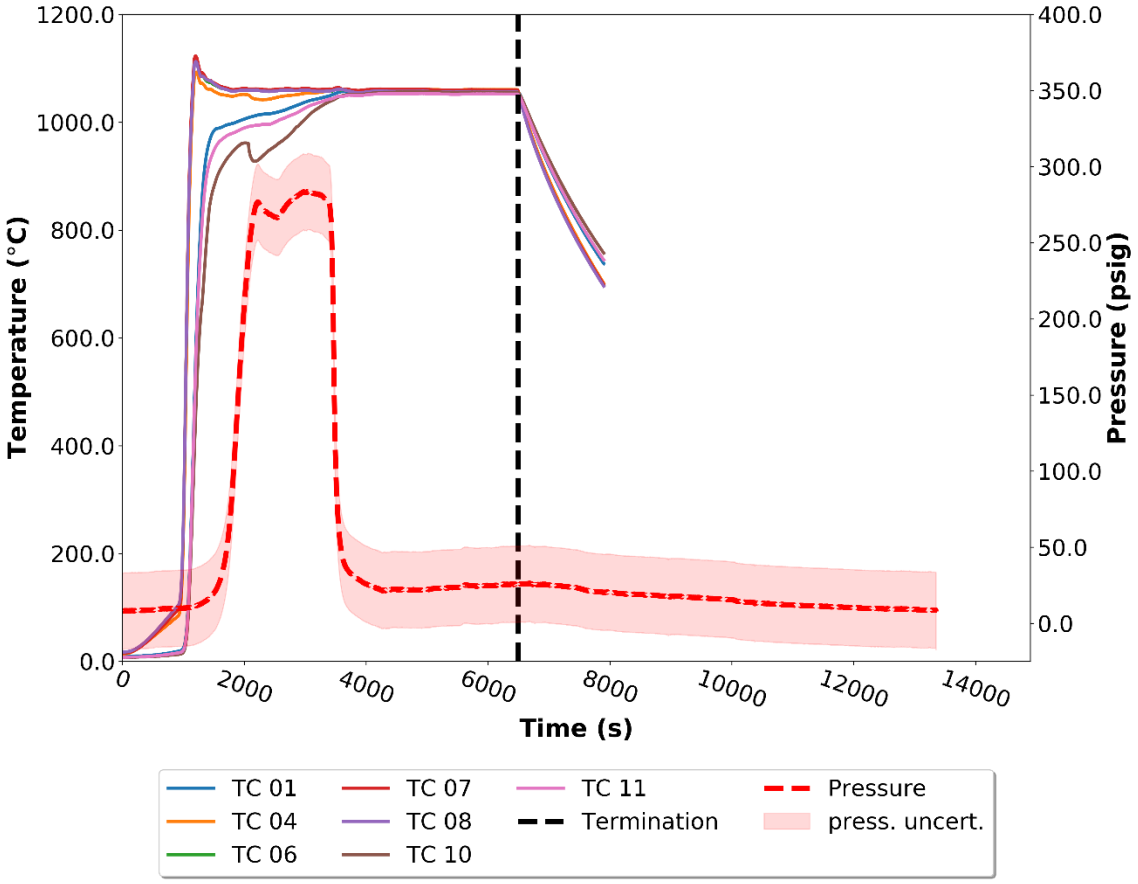

Figure 4-6. Temperature and pressure for Sequence 3.

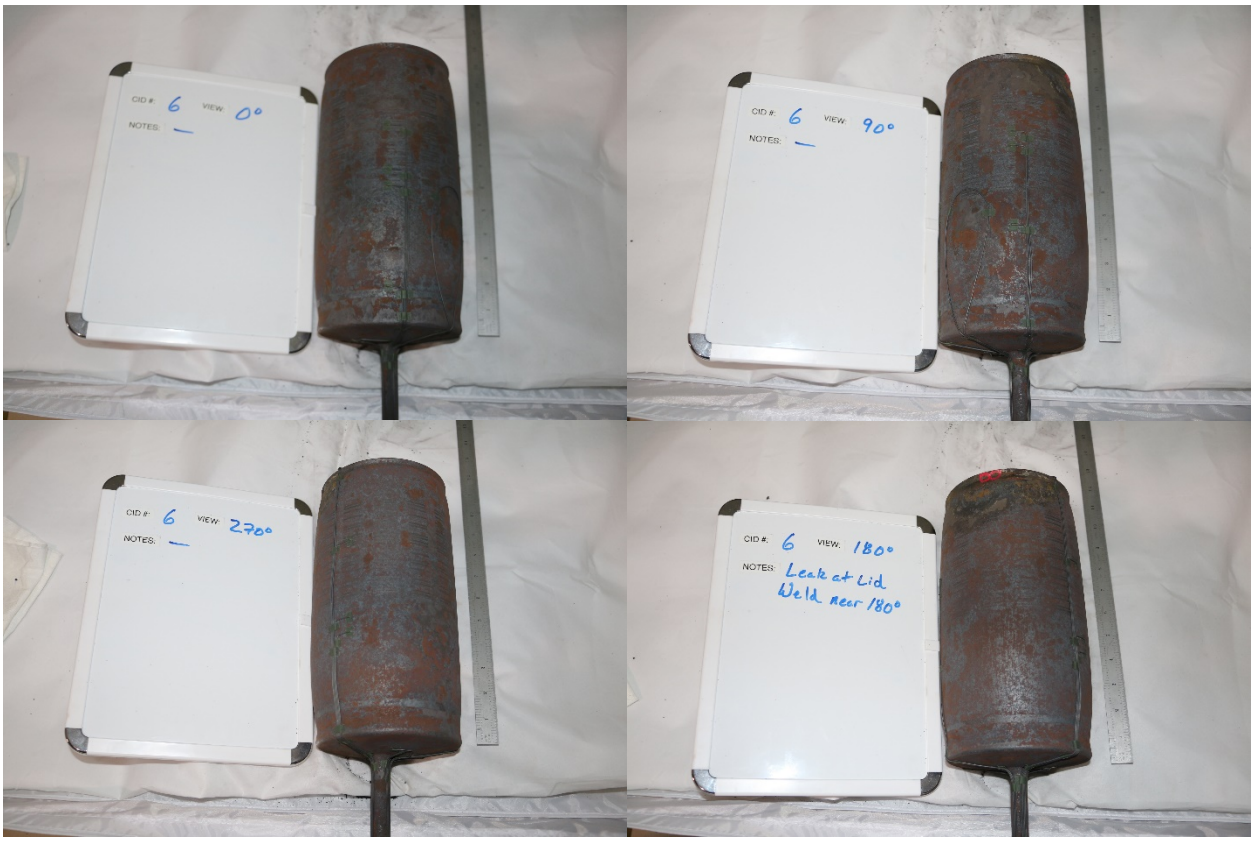

Figure 4-7. Post-test conditions of test vessel for Sequence 3. Angle positions refer to the visible portion of the vessel (see Figure 2-4). Angular positions, in clockwise direction, starting from upper left quadrant: 0°, 90°, 180°, and 270°.

4.4. Sequence 4: CID-10

In Sequence 4, the tested outer 3013 container version was switched to the Flowform version. The payload conditions and heating profile used were the same as those in Sequence 2, where the vessel contained 12 g of H_2O but no salt. The heating profile used was the ASTM-E1529 profile. The thermal and pressure response for Sequence 4 are captured in Figure 4-8, and the post-test conditions of the vessel are captured in Figure 4-9.

Figure 4-8 shows how the Flowform configuration responded differently from the EPD configuration when comparing to Figure 4-3 (Sequence 2). Specifically, Sequence 4 experienced a much larger pressurization and an obvious breach (abrupt depressurization) when compared to Sequence 2. The peak pressurization in Sequence 4 was 324 ± 25 psig at 2630 seconds, which is just over 200 psi ± 50 above the peak pressure experienced by the vessel in Sequence 2. Then, just before 2900 seconds into the test, a breach was observed by the vessel as noted by the sudden pressure drop in the figure. Figure 4-10 shows how the expelled gases ignited with the incident heat just after the vessel was breached. This flame is indicative of reactions occurring within the payload before the breach that possibly led to the generation of combustible gases (such as hydrogen) produced from the heat-up of the payload. Since the payloads were nearly identical between Sequence 2 and Sequence 4, the different results suggest that the manufacturing process and differences between the inner container and convenience container designs significantly influences the mechanical response of the 3013 container in a fire accident scenario. The test was allowed to continue until 3780 seconds, at which point power to the heaters was terminated. Post-test leak checks identified the vessel breach to be near the 100° point in the axial center of the vessel (see red mark in Figure 4-9, 180° image), and the measured mass loss for the vessel was ~48 grams. Approximate measurements to capture swelling of the vessel showed the vessel increased ~1.85 cm in length and ~3.9 cm in diameter at the sites of maximum deformation.

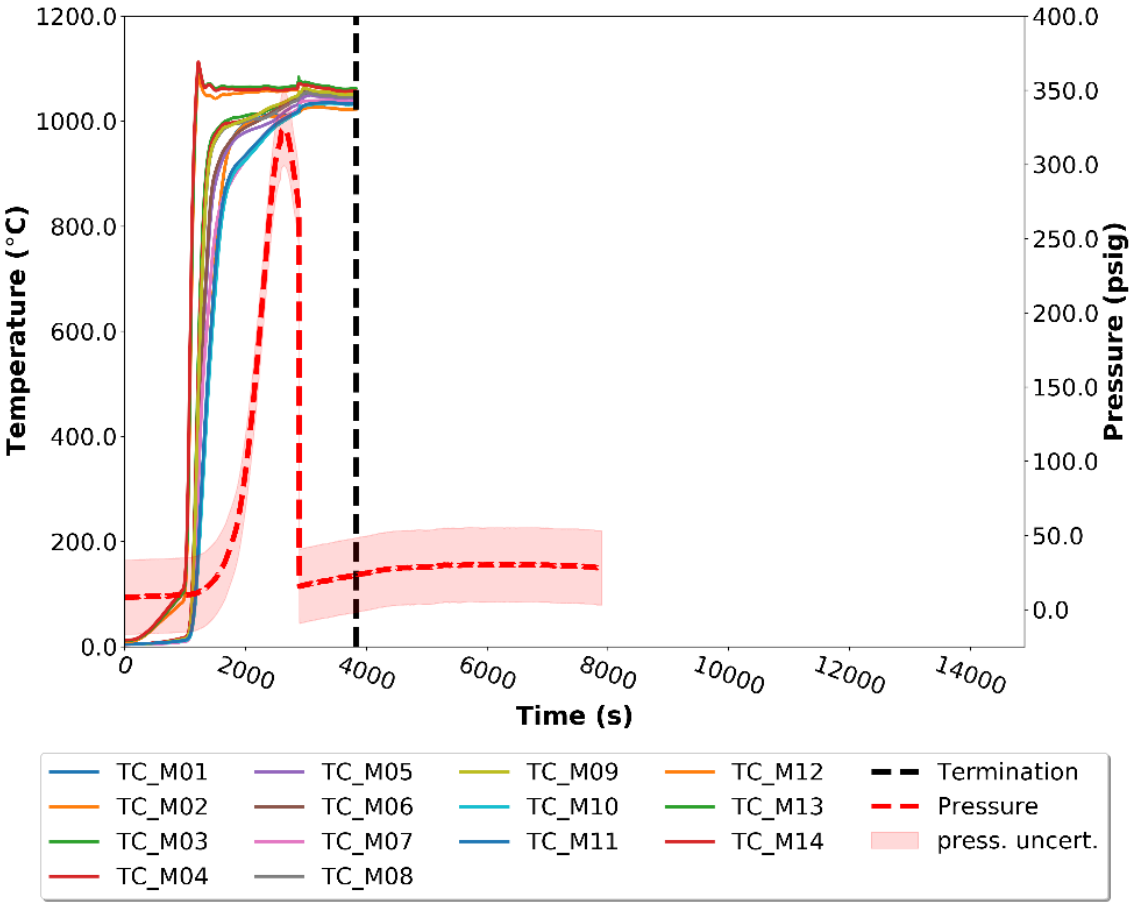

Figure 4-8. Temperature and pressure for Sequence 4.

Figure 4-9. Post-test conditions of test vessel for Sequence 4. Angle positions refer to the visible portion of the vessel (see Figure 2-4). Angular positions, in clockwise direction, starting from upper left quadrant: 0°, 90°, 180°, and 270°.

Figure 4-10. Exterior view of Sequence 4 during test, immediately after vessel was breached.

4.5. Sequence 5: CID-12

Sequence 5 also exposed a Flowform version of the outer 3013 container to the ASTM-E1529 heating profile. Sequence 5 was different from Sequence 4 in the way Sequence 3 differed from Sequence 2: the payload contained 12 g of H_2O and 928.5 g of salt. The thermal and pressure response for Sequence 5 are captured in Figure 4-11, and the post-test conditions of the vessel are captured in Figure 4-12.

Compared to Sequence 4, when salt was absent in the payload, the peak pressure experienced by Sequence 5 was approximately 10 ± 50 psi higher with an observed peak pressure of 332 ± 25 psig near 2100 seconds. Compared to Sequence 3, where the payload was the same but with the EPD vessel configuration, Sequence 5 saw a pressurization that was approximately 50 ± 50 psi higher. Like the comparison between Sequence 2 and Sequence 4, the different outcomes between Sequence 5 and Sequence 3 support the argument that the manufacturing process and differences between the internal containers influence the mechanical response of the outer 3013 containers in a fire accident scenario. At approximately 2460 seconds, a breach was experienced by the vessel as noted by the sudden pressure drop in Figure 4-11. Figure 4-12 reveals how the vessel significantly deformed as a result of the test, and Figure 4-13 shows how the expelled gases ignited with the incident heat just after the vessel was breached, similar to Sequence 4. This test was allowed to continue until 3240 seconds, at which point power to the heater was terminated. Post-test leak checks identified the vessel breach to be near the 200° position about six inches from the bottom of the unit (see red mark in Figure 4-12, 180° image), and the measured mass loss for the vessel was ~5 grams. Approximate measurements to capture swelling of the vessel showed the vessel increased ~1.8 cm in length and ~3.0 cm in diameter at the sites of maximum deformation.

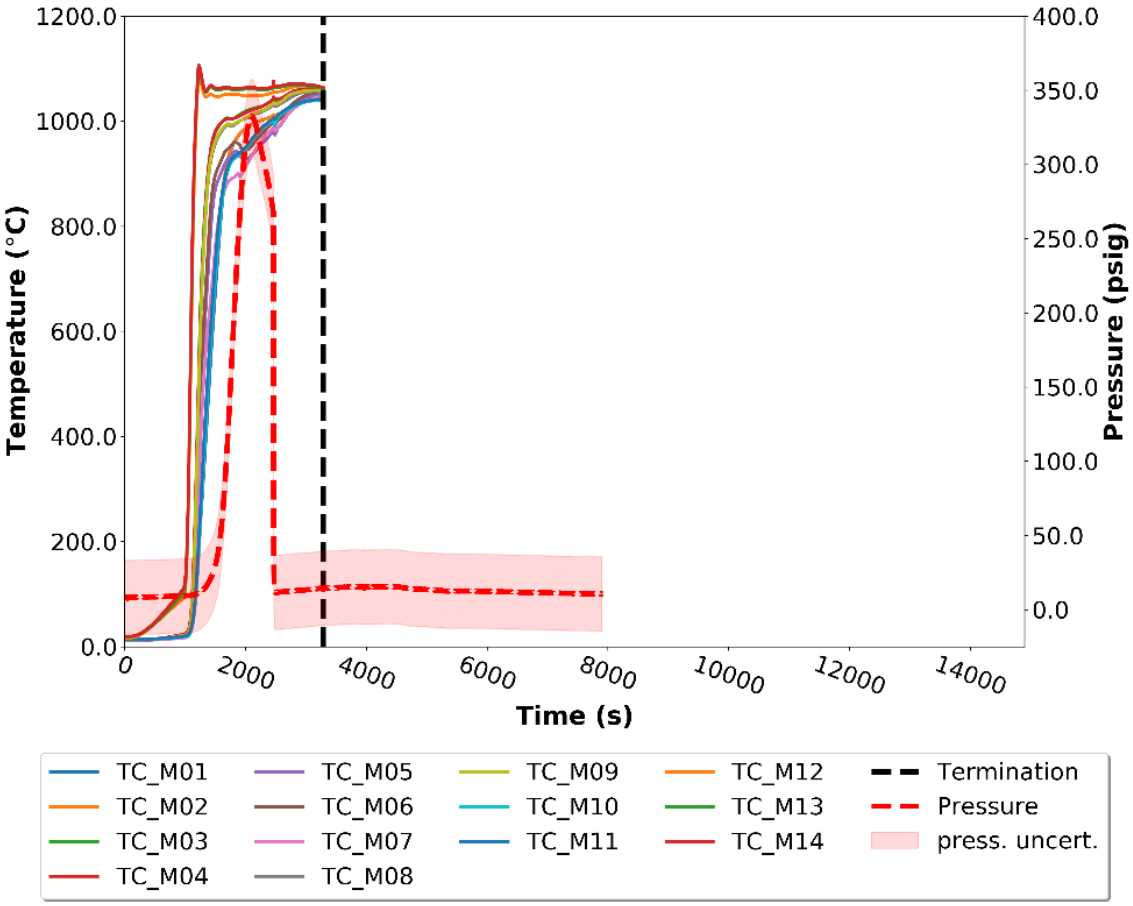

Figure 4-11. Temperature and pressure for Sequence 5.

Figure 4-12. Post-test conditions of test vessel for Sequence 5. Angle positions refer to the visible portion of the vessel (see Figure 2-4). Angular positions, in clockwise direction, starting from upper left quadrant: 0°, 90°, 180°, and 270°.

Figure 4-13. Exterior view of Sequence 5 during test, immediately after vessel was breached.

4.6. Sequence 6: CID-4

Sequence 6 marked the departure from the previous four tests in that the payload contained a lower amount of H_2O at 6 g instead of 12 g. The outer container was an EPD version, no salt was included in the payload, and the heating profile used was the ASTM-E1529. The thermal and pressure response for Sequence 6 are captured in Figure 4-14, and the post-test conditions of the vessel are captured in Figure 4-15.

Figure 4-14 shows how the vessel response was similar to Sequence 2, where the test conditions were comparable except for the payload instead including 12 g of H_2O. The peak pressurization in Sequence 6, however, was larger than Sequence 2 despite the lower moisture. At 3789 seconds, the vessel experienced the peak pressure of 186 ± 25 psig, which is ~63 ± 50 psi over the peak pressure experienced by Sequence 2 despite the lower moisture in CID-4. SNL performed pre- and post-test calibration checks on the transducers to investigate any unexpected anomalies that could have led to the higher pressure reading in Sequence 6. The operating conditions of the data acquisition system were verified along with temperatures near the pressure transducers to check for unexpected drift. None of the checks that SNL performed indicated that anything went wrong with the test or the data acquisition process to have skewed the data.

Figure 4-14 also shows how the pressure gradually decreased after reaching this peak until the end of the test, which was the full four hours. Post-test leak checks showed that no breach was detected on the vessel using an acceptance criterion of no leaks greater than 1.0×10^{-7} scc/s. Similar to Sequence 2, some deformation was observed around the lid region, and a mass loss of ~38 g was recorded. Again, due to the pressure drop observed, it is possible that the vessel could have experienced loss of hydrogen through diffusion out of the container [16]. Due to the scope of these tests, the

volume increase resulting from the deformation was not measured for this vessel either, so pressure loss from volume expansion alone could not be isolated. Deformed vessel dimensions were not measured for this vessel.

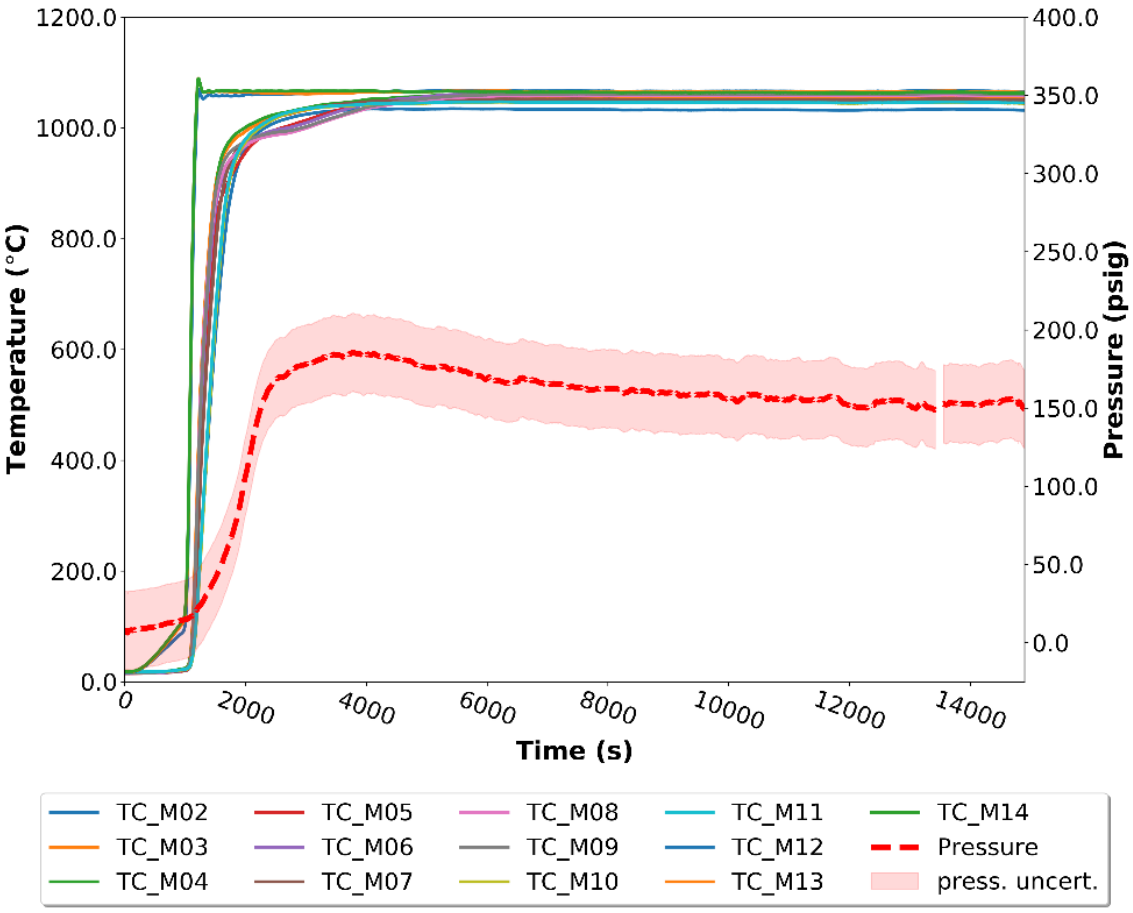

Figure 4-14. Temperature and pressure for Sequence 6.

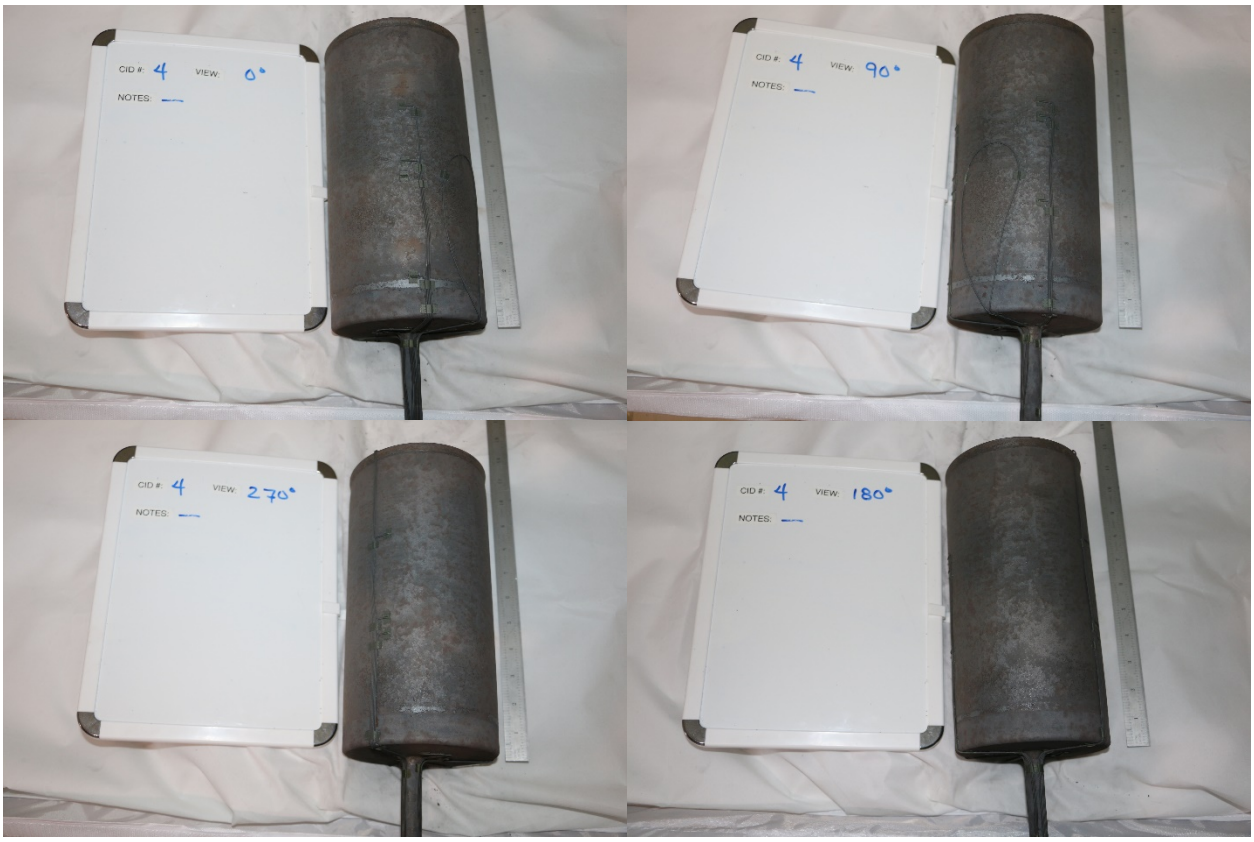

Figure 4-15. Post-test conditions of test vessel for Sequence 6. Angle positions refer to the visible portion of the vessel (see Figure 2-4). Angular positions, in clockwise direction, starting from upper left quadrant: 0°, 90°, 180°, and 270°.

4.7. Sequence 7: CID-5

Sequence 7 was also an EPD container with 6 g of H_2O, but 463.8 g of salt were included in the payload. The heating profile used was the ASTM-E1529. Sequence 7 differed from Sequence 6 in the added salt, and it differed from Sequence 3 in the total amount of moisture and salts. The thermal and pressure response for Sequence 7 are captured in Figure 4-16, and the post-test conditions of the vessel are captured in Figure 4-17. It is important to note that the NQA-1 pressure transducer signal was lost in the middle of the test, therefore Figure 4-16 shows the non-NQA-1 pressure data recorded by SNL's TTC data acquisition system. A non-conformance report (NCR) was filed in the QA package to document this issue (NCR #4). The NCR discusses how the pressure data acquired from SNL's TTC system was generally comparable to (and within the uncertainty bounds of) the MIDAS data, therefore making the substitution of the pressure data permissible. Furthermore, all procedures followed to ensure quality on the MIDAS acquisition systems were also followed for the TTC's transducer and data acquisition system. Unlike the pressure transducer connected to the MIDAS data acquisition system, the TTC pressure transducer had a range up to 1000 psig and an uncertainty of ±5 psi, which is reflected in the figure.

Figure 4-16 shows how the vessel response in this test compared to Sequence 3 and Sequence 6. Peak pressurization of Sequence 7 was 229 ± 5 psig at 3430 seconds, which was 43 ± 30 psi higher than Sequence 6 but 55 ± 30 psig lower than Sequence 3. While sudden but not as abrupt as Sequence 3, the pressure dropped at ~6050 seconds in a manner indicative of a breach. However, this test also ran for the full four hours because the pressure did not drop to near ambient as the previous container failures had (Sequences 3, 4, and 5), and there was a possibility that the pressure drop was not a breach. Post-test leak checks showed that a breach was detected at the 300° position along the lid weld, which is captured in the 300° image of Figure 4-17. While post-test volume change was not measured, visual inspection of Figure 4-17 also shows significant deformation when compared to Sequence 6 and comparable deformation when compared to Sequence 3. Unlike Sequences 3 and 6, however, no mass loss was detected in Sequence 7. Approximate measurements to capture swelling of this vessel showed the vessel increased ~2.4 cm in length and ~0.7 cm in diameter at the sites of maximum deformation.

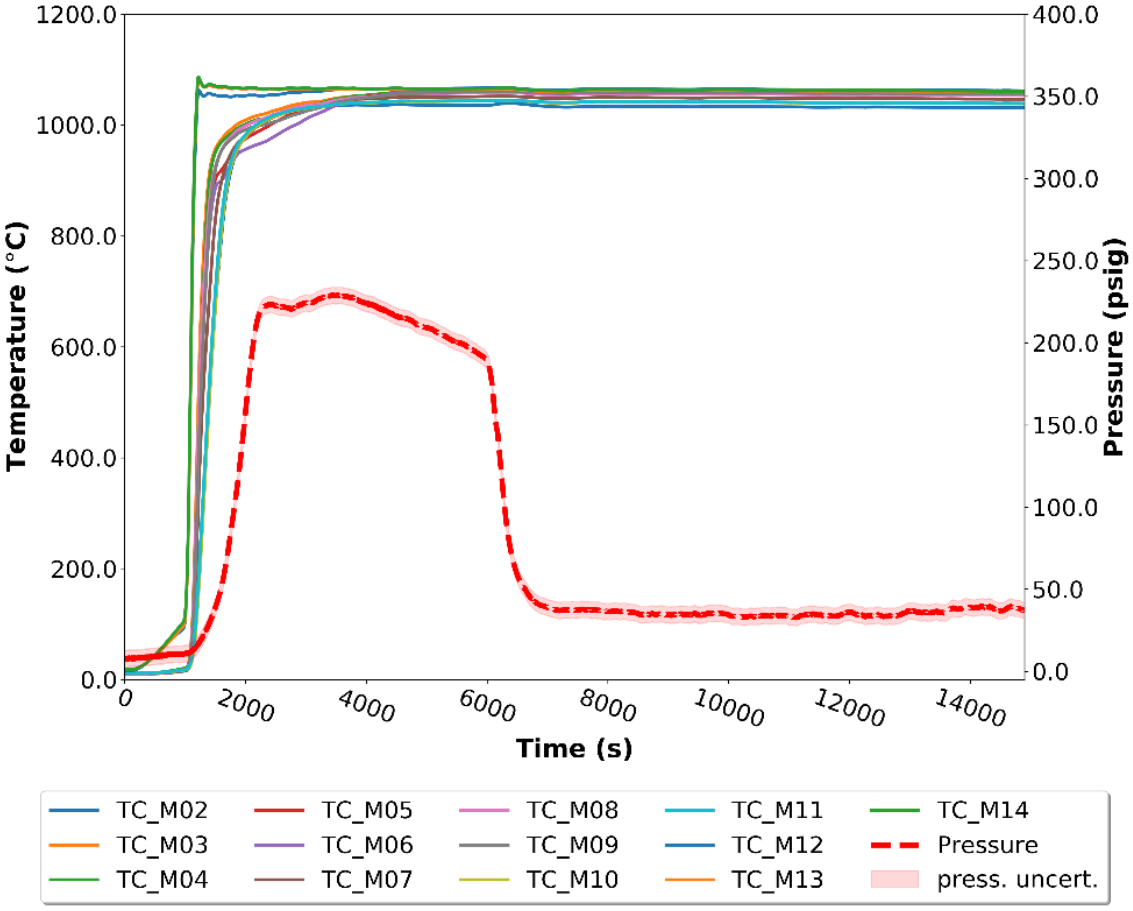

Figure 4-16. Temperature and pressure for Sequence 7. Shaded region around pressure is instrument uncertainty

Figure 4-17. Post-test conditions of test vessel for Sequence 7. Angle positions refer to the visible portion of the vessel (see Figure 2-4). Angular positions, in clockwise direction, starting from upper left quadrant: 0°, 90°, 180°, and 300°.

4.8. Sequence 8: CID-8

Sequence 8 was a Flowform version of the outer container with 6 g of H_2O and no salt in the payload. The heating profile used was the ASTM-E1529 profile. Sequence 8 was similar to Sequence 6 with the only difference being the outer container type. Sequence 8 was also comparable to Sequence 4 in that it was a Flowform version of the container with moisture and no salt in the payload, but Sequence 8 only contained 6 g of moisture (compared to 12 g in Sequence 4). The thermal and pressure response for Sequence 8 are captured in Figure 4-18, and the post-test conditions of the vessel are captured in Figure 4-19.

Figure 4-18 shows how the vessel response in this test compared to Sequence 4 and Sequence 6. Peak pressurization of Sequence 8 was 244 ± 25 psig at 2899 seconds, which was 80 ± 50 psi lower than Sequence 4 but 58 ± 50 psi higher than Sequence 6. The pressure gradually dropped until reaching a breaching point at 4840 seconds. Due to this breach, this test was terminated at 6660 seconds even though the pressure did not drop to ambient because similar performance in the previous test had been documented to have a breach. Post-test leak checks showed that a breach was detected near the 0° position along the axial center, and this is captured in the 0° image of Figure 4-19. While post-test volume change was not measured, visual inspection of Figure 4-19 also shows significant deformation when compared to Sequence 6 and slightly less deformation when

compared to Sequence 4. A mass loss of 10 g showed that the Flowform container in Sequence 8 lost less mass than the EPD equivalent (Sequence 6) and the Flowform version having comparable composition but higher moisture (Sequence 4). Approximate measurements to capture swelling of the vessel showed the vessel increased ~2.0 cm in length and ~3.25 cm in diameter at the sites of maximum deformation.

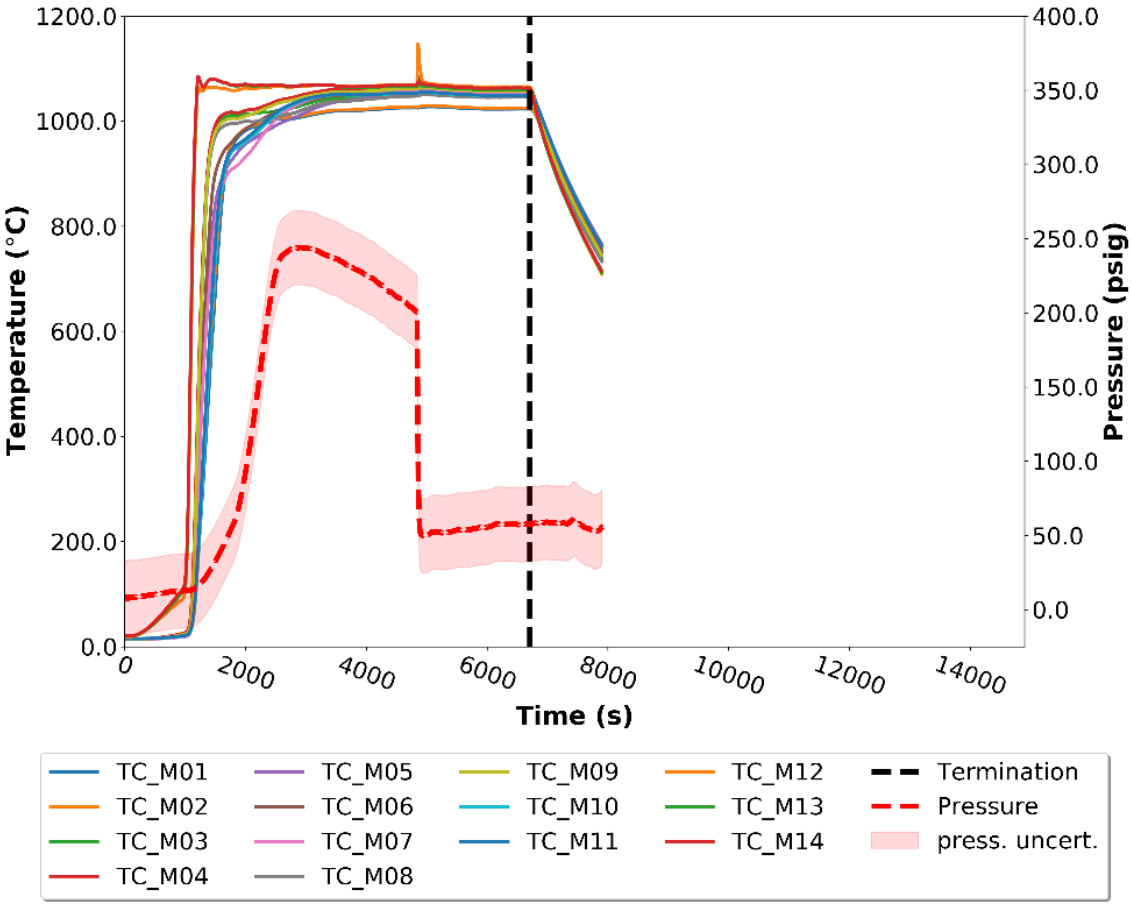

Figure 4-18. Temperature and pressure for Sequence 8.

Figure 4-19. Post-test conditions of test vessel for Sequence 8. Angle positions refer to the visible portion of the vessel (see Figure 2-4). Angular positions, in clockwise direction, starting from upper left quadrant: 0°, 90°, 180°, and 270°.

4.9. Sequence 9: CID-11

Sequence 9 was a Flowform version of the outer container with 6 g of H_2O and 463.8 g of salt in the payload. The heating profile used was the ASTM-E1529 profile. Sequence 9 tested the same payload composition as Sequence 7, but the outer container version was the Flowform instead of the EPD. Sequence 9 was also similar to Sequence 8 in testing the Flowform outer container version with lower moisture, but Sequence 9 contained the added salt in the payload. The thermal and pressure response for Sequence 9 are captured in Figure 4-20, and the post-test conditions of the vessel are captured in Figure 4-21.

Figure 4-20 shows the vessel's thermal and pressure response for Sequence 9. The response can be compared to Sequence 7 and Sequence 8. Peak pressurization of Sequence 9 was 253 ± 25 psig at 2251 seconds, which was 24 ± 30 psi higher than Sequence 7 and 9 ± 50 psi higher than Sequence 8. The pressure gradually dropped until reaching a breaching point at 3975 seconds. Due to this breach showing no signs of re-pressurization, this test was terminated at 5220 seconds. Post-test leak checks showed that a breach was detected near the 110° position along the axial center, and this is captured in the 90° and 180° images of Figure 4-21. While post-test volume change was not measured, visual inspection of Figure 4-21 also shows significant deformation when compared to Sequence 7 and comparable deformation when compared to Sequence 8. A mass loss of 19 g showed that this test lost more mass than Sequences 7 and 8. When compared to Sequence 5, which was the same outer container version with added salt and moisture but in lower quantities, the peak pressurization was 81 ± 50 psi lower but the mass loss was ~14 g higher. Approximate measurements to capture swelling of the vessel showed the vessel increased ~1.75 cm in length and ~4.2 cm in diameter at the sites of maximum deformation.

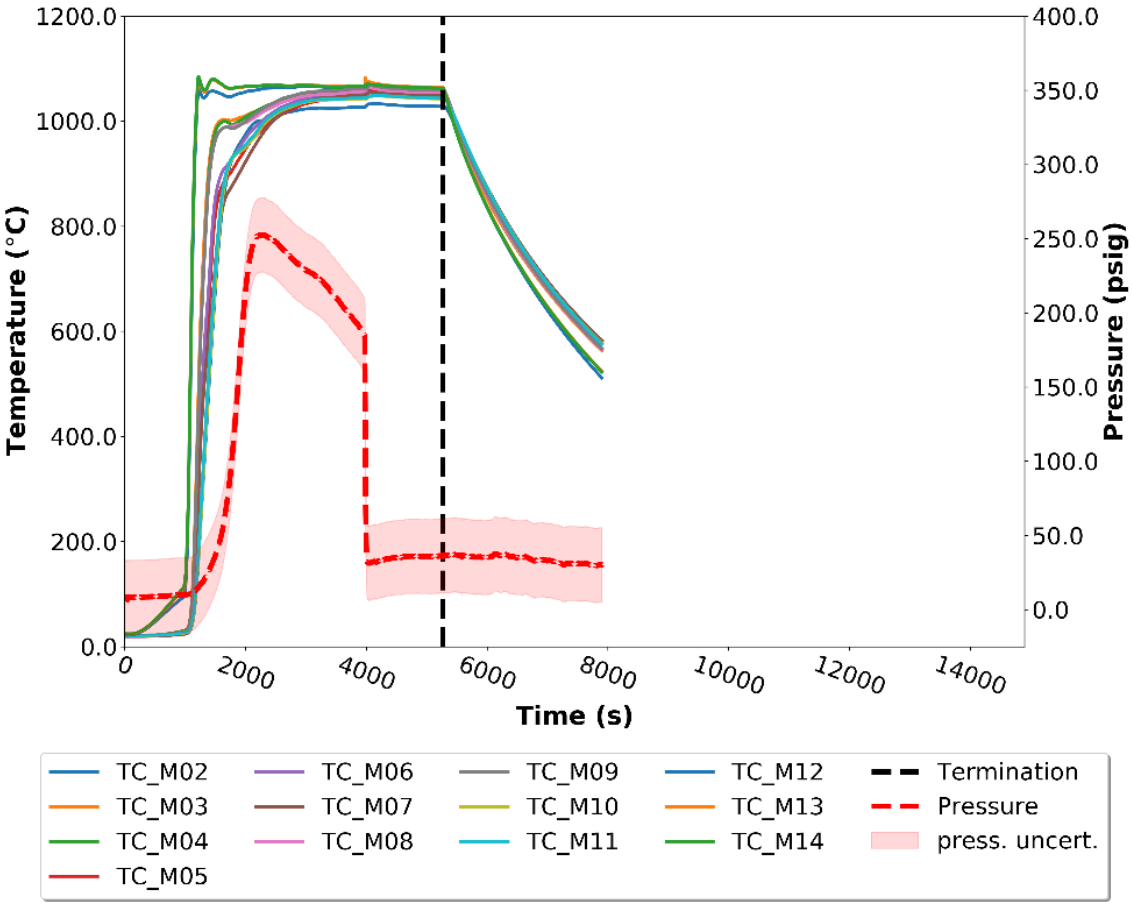

Figure 4-20. Temperature and pressure for Sequence 9.

Figure 4-21. Post-test conditions of test vessel for Sequence 9. Angle positions refer to the visible portion of the vessel (see Figure 2-4). Angular positions, in clockwise direction, starting from upper left quadrant: 0°, 90°, 180°, and 270°.

4.10. Sequence 10: CID-9

After exposing Sequences 2 through 9 with the ASTM-E1529 heating profile, Sequence 10 exposed the test subject to ASTM-E119m. Sequence 10 was also a Flowform version of the outer container with 6 g of H_2O and no salt in the payload. Sequence 10 tested the same payload composition as Sequences 6, but the outer container version was the Flowform instead of the EPD. By the same token, Sequence 10 tested the same payload and container type as Sequence 8 but exposed the test subject to the ASTM-E119m heating curve instead. Compared to Sequence 1 where the ASTM-E119m heating profile was also used, Sequence 10 varied in the container version used and in the amount of moisture, where Sequence 10 only contained 6 g of moisture instead of the 18 g in Sequence 1. The thermal and pressure response for Sequence 10 are captured in Figure 4-22, and the post-test conditions of the vessel are captured in Figure 4-23.

Figure 4-22 shows how the vessel response had some similarities to Sequence 1. Peak pressurization of Sequence 10 was 262 ± 25 psig, and this occurred at the end of the four-hour criterion as the pressure was still slowly but steadily rising at that point. Sequence 1 had a similar pressure response, except that there was a slow pressure decline by the end of the test and peak pressurization was only at 169 ± 25 psig. This higher pressurization occurred despite the higher moisture content in Sequence 1, but it was consistent with prior tests revealing that the Flowform version of the outer container generally experienced larger pressurizations under comparable conditions. Compared to Sequence 8, which was an identical vessel but tested with the ASTM-E1529 heating profile, Sequence 10 saw a peak pressure that was 18 ± 50 psig higher. When making comparisons, however, it should be noted that this peak pressurization in Sequence 10 was experienced at the end of the test and with no noticeable breach (unlike Sequence 8 that experienced a peak pressure and breach relatively early in the test). Due to the pressure profile being observed to continue increasing at the end of the test, post-test leak checks were not performed. Similar to Sequence 1, Figure 4-23 shows how no visible deformation was noticed for the vessel in Sequence 10 after test exposure. Interestingly, a mass gain of 8 grams was recorded for the vessel in Sequence 10. This increase in mass could have resulted from debris collected on the bottom of the shroud since it was added as part of the post-test mass (see Figure 4-24). Collection of this debris was initiated in Sequence 2, so any debris collected in Sequence 1 was not considered and therefore cannot be compared. However, since Sequence 1 recorded zero mass loss, any debris added would have similarly resulted in a net mass gain. With regards to swelling and similar to the vessel in Sequence 1, minimal deformation was recorded in the vessel for Sequence 10. Approximate measurements to capture swelling of the vessel showed that the vessel increased ~.02 cm in length and ~0.1 cm in diameter at the sites of maximum deformation.

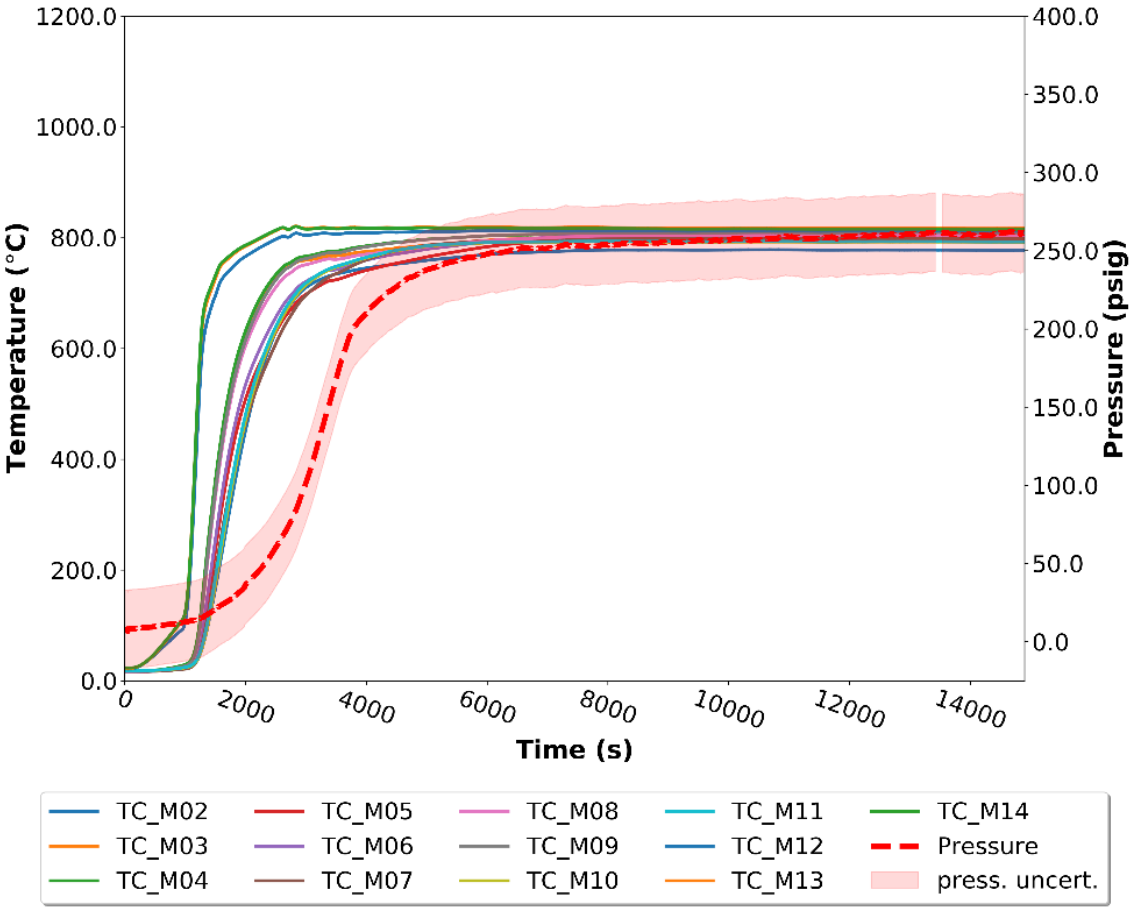

Figure 4-22. Temperature and pressure for Sequence 10.

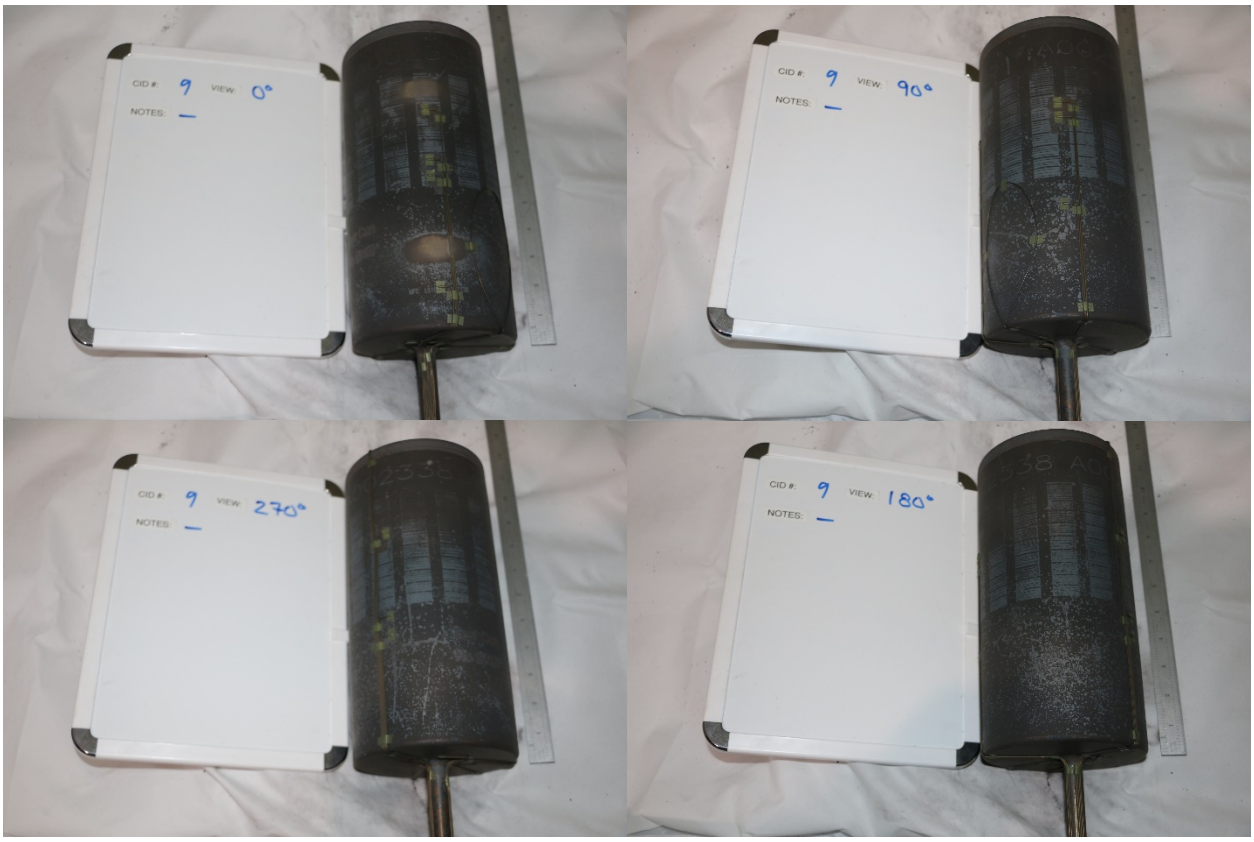

Figure 4-23. Post-test conditions of test vessel for Sequence 10. Angle positions refer to the visible portion of the vessel (see Figure 2-4). Angular positions, in clockwise direction, starting from upper left quadrant: 0°, 90°, 180°, and 270°.

Figure 4-24. Post-test image of Sequence 10 showing debris from shroud collected at the bottom of the shroud.

5. SUMMARY

Sandia National Laboratories (SNL) and Savannah River Site (SRS) carried out a test campaign to characterize the fire-induced pressure response for the two versions of the DOE-STD-3013 assembly when filled with representative payloads; (1) the ARIES Flowform Set Long Term Storage Assembly version and (2) the EPD Set 3013 Package Assembly version. The test campaign specifically aimed to determine and characterize whether the container would fail under bounding fire conditions when payload constituents were conservatively chosen. Failure specific characteristics of interest were: (1) the container pressure response throughout a test, (2) the evolution of container temperature throughout a test, and (3) failure type if the vessels were breached during a test. A total of 10 tests were executed, the results of which are discussed in this report.

The expected fire response conditions for 3013 containers were bounded with 2 heating profiles in this test campaign: ASTM-E1529, which represents exposure in and engulfing pool fire and a modified version of ASTM-E119, representing an impinging ordinary combustible fire or bounding room fire conditions. Between the two heating profiles, ASTM-E1529 resulted in larger pressurizations and thus produced more conservative outcomes. As a result, 8 out of the 10 tests were tested using the ASTM-E1529 heating profile.

Within each container version, there was a variation of the composition of the payload as defined in *Recommended 3013 Loadings and Configurations for Fire Testing* [17]. Aluminum oxide (Al2O3), water (H2O), Salts (NaCl, CaCl2, KCl), stainless steel spacers, and a free volume of gas (He/air) comprised the different payloads. For the water content, either of three quantities were combined with the payload: 18 grams, 12 grams, or 6 grams of moisture. The salts added to some of the containers were to investigate the effects of high-temperature corrosion, and thus to determine whether the presence of salts affect the response and performance of a 3013 container in a fire scenario. Overall, the payload was designed so that the free gas volume in each test vessel bounded the minimum free gas volume of the containers in inventory.

Out of the 10 tests, six experienced some type of breach. For those tests exposed to the ASTM-E119m curve, no breach points were found in either test. Peak pressures experienced by the vessels ranged between 123 $\pm$ 25 psig and 332 $\pm$ 25 psig. For those tests exposed to the ASTM-E1529 curve, only those vessels that experienced pressures over 200 psig were found to have been breached. All vessels with added salts pressurized more than their no-salt counterparts and also experienced a breach, independent of the outer container version. For those vessels without added salts, only those tests on the Flowform version of the outer container were found to have been breached. The EPD containers with no added salts did not experience a breach, independent of the amount of moisture in the vessel or the fire test temperature. In all cases where the container failed, the failure pressures were more than an order of magnitude less than the failure pressures seen in the ambient temperature hydro tests. This is to be expected since stainless steel strength decreases with temperature. In addition, all breach points observed were small and required helium leak testing to locate. Lastly, for any given set of conditions, the Flowform configurations experienced higher peak pressures under comparable heating and payload conditions.

6. REFERENCES

[1] U.S. Department of Energy, "Airborne Release Fractions/Rates and Respirable Fractions for non-Reactor Nuclear Facilitites: Volume 1 - Analysis of Experimental Data," U.S. Department of Energy, Washington, D.C., 1994.

[2] Los Alamos National Lab, "Designing a container for safe, long-term storage: A primer on the DOE 3013 Standard," [Online]. Available: https://www.lanl.gov/orgs/nmt/nmtdo/AQarchive/04fall/primer.html. [Accessed 05 01 2021].

[3] H. Mendoza , A. R. Baird, V. Figueroa and W. Gill, *PCV/SCV/3013 Thermal Test Program Phase 3 Test Plan Rev. 0,* Sandia National Laboratories, 2020.

[4] H. Mendoza, W. Gill, R. Sprankle, A. Shefferman, V. G. Figueroa and S. Sanborn, "Fire-Induced Pressure Response and Failure Charcterization of PCV/SCV/3013 Containers - Phase 1: SAND2019-7311," Sandia National Laboratories, Albuquerque, NM, 2019.

[5] J. E. Narlesky, C. W. Emms, D. C. Tung, J. T. Stritzinger, D. J. Gregory, K. P. Deike, S. Apgar, A. M. Barraza, K. M. Hansel, L. Lopez, T. J. Madrid, A. Noonan and Thornburg, "LANL Phase 3 Container Loading in Support of the Fire-Induced PressureResponse and Failure Characterization of PCV/SCV/3013 Containers," Los Alamos National Laboratory, Los Alamos, NM, 2020.

[6] U.S Department of Energy, "DOE-STD-3013-2018," U.S. Department of Energy, Washington, DC, 2018.

[7] S. Hensel and R. A. Sprankle, "Recommended 3013 Loadings and Configurations for Fire Testing," SRNS-E1900-2019-00005, 2019.

[8] D. K. Veirs, J. McClard and S. Hensel, "Calculation of fill and filler masses and volumes for 3013 fire test," Los Alamos National Laboratory, 2019.

[9] Savannah River Site, *MODIFY 3013 CONTAINER FOR TESTING AT SNL: WO:01707060,* Savannah River Site, 2020.

[10] K. C. Neikirk, *Loaded 3013 w/ Manifold Assembly Fabrication, Pressure Testing, Leak Testing, and Clearning at SRS,* Savannah River National Laboratory, 2021.

[11] Sandia National Laboratories, "Quality Assurance Program Plan Mobile Instrumentation Data Acquisition System Upgrade," Sandia National Laboratories, 2014.

[12] Gefran , "Gefran: Beyond Technology," [Online]. Available: https://www.gefran.com/en/products/222-kn-nak-sodium-potassium-voltage-output. [Accessed 28 December 2020].

[13] American Society for Testing and Materials, "Standard Test Methods for Fire Tests of Building Construction and Materials," ASTM, 2018.

[14] American Society of Testing and Materials, "Standard Test Methods for Determining Effects of Large Hydrocarbon Pool Fires on Structural Members and Assemblies," ASTM, 2014.

[15] A. R. Baird, W. Gill, H. Mendoza and V. Figueroa, "Correlating Incident Heat Flux and Source Temperature to Meet ASTM-E1529 Requirements for RAM Packaging Components Thermal Testing," in *Pressure Vessels & Piping Conference*, 2021.

[16] C. San Marchi, B. P. Somerday and S. L. Robinson, "Permeability, solubility and diffusivity of hydrogen isotopes in stainlesss steels at high gas pressures," *International Journal of Hydrogen Energy,* vol. 32, pp. 100-116, 2007.

[17] S. J. Hensel and R. A. Sprankle, *Recommended 3013 Loadings and Configurations for Fire Testing,* Savannah River Site, 2019.

7. APPENDIX

7.1. Gas Sample Summary

CID2 GS1 (Prior to Leak Testing)				CID2 GS2 (Post Leak Testing)				CID2 GS3 (Post Thermal Testing)			
Analyte	Quantitation	AMU	Date	Analyte	Quantitation	AMU	Date	Analyte	Quantitation	AMU	Date
Hydrogen	85 ppm	2	11/25/2020 15:32	Hydrogen	58 ppm	2	12/11/2020 15:16	Hydrogen	8.49%	2	11/25/2020
Helium	23.9%	4	11/25/2020 15:32	Helium	55.1%	4	12/11/2020 15:16	Helium-3	15 ppm	3	11/25/2020
Water	94 ppm	18	11/25/2020 15:32	Water	1.19%	18	12/11/2020 15:16	Helium	86.1%	4	11/25/2020
Nitrogen	60.1%	28	11/25/2020 15:32	Nitrogen	31.3%	28	12/11/2020 15:16	Water	811 ppm	18	11/25/2020
Oxygen	15.3%	32	11/25/2020 15:32	Oxygen	8.25%	32	12/11/2020 15:16	Nitrogen	4.74%	28	11/25/2020
Argon	7229 ppm	40	11/25/2020 15:32	Argon	4.09%	40	12/11/2020 15:16	Oxygen	15 ppm	32	11/25/2020
Carbon Dioxide	239 ppm	44	11/25/2020 15:32	Carbon Dioxide	152 ppm	44	12/11/2020 15:16	Argon	6,167 ppm	40	11/25/2020
								Carbon Dioxide	21 ppm	44	11/25/2020
								Other	54 ppm	N/A	11/25/2020
CID3 GS1 (Prior to Leak Testing)				**CID3 GS2 (Post Leak Testing)**				**CID3 GS3 (Post Thermal Testing)**			
Analyte	Quantitation	AMU	Date	Analyte	Quantitation	AMU	Date	Analyte	Quantitation	AMU	Date
Hydrogen	61 ppm	2	11/19/2020 14:53	Hydrogen	35 ppm	2	11/19/2020 15:20	Hydrogen	40.9%	2	5/11/2021 3:13
Helium	33.60%	4	11/19/2020 14:53	Helium	59.10%	4	11/19/2020 15:20	Helium	37.8%	4	5/11/2021 3:13
Water	0 ppm	18	11/19/2020 14:53	Water	0 ppm	18	11/19/2020 15:20	Water	441 ppm	18	5/11/2021 3:13
Nitrogen	51.40%	28	11/19/2020 14:53	Nitrogen	31.80%	28	11/19/2020 15:20	Nitrogen	19.7%	28	5/11/2021 3:13
Oxygen	14.30%	32	11/19/2020 14:53	Oxygen	8.69%	32	11/19/2020 15:20	Oxygen	31 ppm	32	5/11/2021 3:13
Argon	5932 ppm	40	11/19/2020 14:53	Argon	3704 ppm	40	11/19/2020 15:20	Argon	2124 ppm	40	5/11/2021 3:13
Carbon Dioxide	157 ppm	44	11/19/2020 14:53	Carbon Dioxide	88 ppm	44	11/19/2020 15:20	Carbon Dioxide	1.3%	44	5/11/2021 3:13
Other	35 ppm	N/A	11/19/2020 14:53	Other	41 ppm	N/A	11/19/2020 15:20	Benzene	43 ppm	78	5/11/2021 3:13
CID4 GS1 (Prior to Leak Testing)				**CID4 GS2 (Post Leak Testing)**				**CID4 GS3 (Post Thermal Testing)**			
Analyte	Quantitation	AMU	Date	Analyte	Quantitation	AMU	Date	Analyte	Quantitation	AMU	Date
Hydrogen	50 ppm	2	12/11/2020 15:40	Hydrogen	43 ppm	2	03/31/2021 14:25	Hydrogen	8.2%	2	04/15/2021 16:07
Helium	58.8%	4	12/11/2020 15:40	Helium	74.4%	4	03/31/2021 14:25	Helium	89.3%	4	04/15/2021 16:07
Water	0 ppm	18	12/11/2020 15:40	Water	18 ppm	18	03/31/2021 14:25	Water	0 ppm	18	04/15/2021 16:07
Nitrogen	32.2%	28	12/11/2020 15:40	Nitrogen	20.2%	28	03/31/2021 14:25	Nitrogen	2.2%	28	04/15/2021 16:07
Oxygen	8.53%	32	12/11/2020 15:40	Oxygen	5.1%	32	03/31/2021 14:25	Oxygen	16 ppm	32	04/15/2021 16:07
Argon	4091 ppm	40	12/11/2020 15:40	Argon	2292 ppm	40	03/31/2021 14:25	Argon	2517 ppm	40	04/15/2021 16:07
Carbon Dioxide	155 ppm	44	12/11/2020 15:40	Carbon Dioxide	57 ppm	44	03/31/2021 14:25	Carbon Dioxide	5 ppm	44	04/15/2021 16:07
CID5 GS1 (Prior to Leak Testing)				**CID5 GS2 (Post Leak Testing)**				**CID4 GS3 (Post Thermal Testing)**			
Analyte	Quantitation	AMU	Date	Analyte	Quantitation	AMU	Date	Analyte	Quantitation	AMU	Date
Hydrogen	65 ppm	2	11/25/2020 14:53	Hydrogen	47 ppm	2	11/25/2020 14:22	Hydrogen	11.4%	2	4/20/2021 12:30
Helium	47.8%	4	11/25/2020 14:53	Helium	68.2%	4	11/25/2020 14:22	Helium	3.7%	4	4/20/2021 12:30
Water	244 ppm	18	11/25/2020 14:53	Water	29 ppm	18	11/25/2020 14:22	Water	484 ppm	18	4/20/2021 12:30
Nitrogen	41.0%	28	11/25/2020 14:53	Nitrogen	25.1%	28	11/25/2020 14:22	Nitrogen	66.9%	28	4/20/2021 12:30
Oxygen	10.6%	32	11/25/2020 14:53	Oxygen	6.4%	32	11/25/2020 14:22	Oxygen	17.1%	32	4/20/2021 12:30
Argon	4839 ppm	40	11/25/2020 14:53	Argon	2957 ppm	40	11/25/2020 14:22	Argon	8066 ppm	40	4/20/2021 12:30
Carbon Dioxide	149 ppm	44	11/25/2020 14:53	Carbon Dioxide	82 ppm	44	11/25/2020 14:22	Carbon Dioxide	2410 ppm	44	4/20/2021 12:30
CID6 GS1 (Prior to Leak Testing)				**CID6 GS2 (Post Leak Testing)**				**CID6 GS3 (Post Thermal Testing)**			
Analyte	Quantitation	AMU	Date	Analyte	Quantitation	AMU	Date	Analyte	Quantitation	AMU	Date
Hydrogen	81 ppm	2	11/25/2020 15:12	Hydrogen	53 ppm	2	11/25/2020 15:56	Hydrogen	35.3%	2	5/11/2021 13:30
Helium	19.6%	4	11/25/2020 15:12	Helium	52.3%	4	11/25/2020 15:56	Helium	5289 ppm	4	5/11/2021 13:30
Water	284 ppm	18	11/25/2020 15:12	Water	28 ppm	18	11/25/2020 15:56	Water	1064 ppm	18	5/11/2021 13:30
Nitrogen	62.9%	28	11/25/2020 15:12	Nitrogen	37.7%	28	11/25/2020 15:56	Nitrogen	51.5%	28	5/11/2021 13:30
Oxygen	16.7%	32	11/25/2020 15:12	Oxygen	9.54%	32	11/25/2020 15:56	Oxygen	11.9%	32	5/11/2021 13:30
Argon	7505 ppm	40	11/25/2020 15:12	Argon	4267 ppm	40	11/25/2020 15:56	Argon	5659 ppm	40	5/11/2021 13:30
Carbon Dioxide	258 ppm	44	11/25/2020 15:12	Carbon Dioxide	163 ppm	44	11/25/2020 15:56	Carbon Dioxide	261 ppm	44	5/11/2021 13:30
								Benzene	46 ppm	78	5/11/2021 13:30

Figure 7-1. Gas Sample Summary for CID2 - CID6

CID8 GS1 (Prior to Leak Testing)				CID8 GS2 (Post Leak Testing)				CID8 GS3 (Post Thermal Testing)			
Analyte	Quantitation	AMU	Date	Analyte	Quantitation	AMU	Date	Analyte	Quantitation	AMU	Date
Hydrogen	98 ppm	2	12/11/2020 14:46	Hydrogen	47 ppm	2	03/31/2021 14:04	Hydrogen	3174 ppm	2	04/26/2021 1000
Helium	26.0%	4	12/11/2020 14:46	Helium	51.6%	4	03/31/2021 14:04	Helium	1032 ppm	4	04/26/2021 1000
Water	1.88%	18	12/11/2020 14:46	Water	6994 ppm	18	03/31/2021 14:04	Water	1.78%	18	04/26/2021 1000
Nitrogen	56.5%	28	12/11/2020 14:46	Nitrogen	37.6%	28	03/31/2021 14:04	Nitrogen	79.6%	28	04/26/2021 1000
Oxygen	14.9%	32	12/11/2020 14:46	Oxygen	9.7%	32	03/31/2021 14:04	Oxygen	17.2%	32	04/26/2021 1000
Argon	6901 ppm	40	12/11/2020 14:46	Argon	4246 ppm	40	03/31/2021 14:04	Argon	9545 ppm	40	04/26/2021 1000
Carbon Dioxide	288 ppm	44	12/11/2020 14:46	Carbon Dioxide	88 ppm	44	03/31/2021 14:04	Carbon Dioxide	516 ppm	44	04/26/2021 1000
CID9 GS1 (Prior to Leak Testing)				**CID9 GS2 (Post Leak Testing)**				**CID9 GS3 (Post Thermal Testing)**			
Analyte	Quantitation	AMU	Date	Analyte	Quantitation	AMU	Date	Analyte	Quantitation	AMU	Date
Hydrogen	92 ppm	2	12/11/2020 15:32	Hydrogen	67 ppm	2	04/07/20201 10:29	Hydrogen	54.8%	2	5/11/2021 13:45
Helium	24.2%	4	12/11/2020 15:32	Helium	55.99%	4	04/07/20201 10:29	Helium	27.2%	4	5/11/2021 13:45
Water	2.27%	18	12/11/2020 15:32	Water	7923 ppm	18	04/07/20201 10:29	Water	5383 ppm	18	5/11/2021 13:45
Nitrogen	52.4%	28	12/11/2020 15:32	Nitrogen	31.25%	28	04/07/20201 10:29	Nitrogen	15.6%	28	5/11/2021 13:45
Oxygen	14.1%	32	12/11/2020 15:32	Oxygen	8.04%	32	04/07/20201 10:29	Oxygen	36 ppm	32	5/11/2021 13:45
Argon	7.05%	40	12/11/2020 15:32	Argon	3.92%	40	04/07/20201 10:29	Argon	1.8%	40	5/11/2021 13:45
Carbon Dioxide	260 ppm	44	12/11/2020 15:32	Carbon Dioxide	74 ppm	44	04/07/20201 10:29	Carbon Dioxide	54 ppm	44	5/11/2021 13:45
								Benzene	46 ppm	78	5/11/2021 13:45
CID10 GS1 (Prior to Leak Testing)				**CID10 GS2 (Post Leak Testing)**				**CID10 GS3 (Post Thermal Testing)**			
Analyte	Quantitation	AMU	Date	Analyte	Quantitation	AMU	Date	Analyte	Quantitation	AMU	Date
Hydrogen	84 ppm	2	11/25/2020 15:20	Hydrogen	86 ppm	2	3/31/2021 14:31	Hydrogen	79 ppm	2	5/11/2021 15:15
Helium	30.0%	4	11/25/2020 15:20	Helium	55.0%	4	3/31/2021 14:31	Helium	ND	4	5/11/2021 15:15
Water	2.65%	18	11/25/2020 15:20	Water	ND	18	3/31/2021 14:31	Water	225 ppm	18	5/11/2021 15:15
Nitrogen	53.2%	28	11/25/2020 15:20	Nitrogen	35.5%	28	3/31/2021 14:31	Nitrogen	77.9%	28	5/11/2021 15:15
Oxygen	13.4%	32	11/25/2020 15:20	Oxygen	9.1%	32	3/31/2021 14:31	Oxygen	21.1%	32	5/11/2021 15:15
Argon	6308 ppm	40	11/25/2020 15:20	Argon	4094 ppm	40	3/31/2021 14:31	Argon	9527 ppm	40	5/11/2021 15:15
Carbon Dioxide	246 ppm	44	11/25/2020 15:20	Carbon Dioxide	84 ppm	44	3/31/2021 14:31	Carbon Dioxide	555 ppm	44	5/11/2021 15:15
CID11 GS1 (Prior to Leak Testing)				**CID11 GS2 (Post Leak Testing)**				**CID11 GS3 (Post Thermal Testing)**			
Analyte	Quantitation	AMU	Date	Analyte	Quantitation	AMU	Date	Analyte	Quantitation	AMU	Date
Hydrogen	53 ppm	2	12/11/2020 15:09	Hydrogen	40 ppm	2	12/11/2020 15:00	Hydrogen	7384 ppm	2	04/29/21 15:00
Helium	54.9%	4	12/11/2020 15:09	Helium	72.0%	4	12/11/2020 15:00	Helium	1535 ppm	4	04/29/21 15:00
Water	148 ppm	18	12/11/2020 15:09	Water	0 ppm	18	12/11/2020 15:00	Water	2487 ppm	18	04/29/21 15:00
Nitrogen	35.0%	28	12/11/2020 15:09	Nitrogen	22.0%	28	12/11/2020 15:00	Nitrogen	83.34%	28	04/29/21 15:00
Oxygen	9.68%	32	12/11/2020 15:09	Oxygen	5.78%	32	12/11/2020 15:00	Oxygen	14.50%	32	04/29/21 15:00
Argon	4378 ppm	40	12/11/2020 15:09	Argon	2637 ppm	40	12/11/2020 15:00	Argon	1.00%	40	04/29/21 15:00
Carbon Dioxide	132 ppm	44	12/11/2020 15:09	Carbon Dioxide	100 ppm	44	12/11/2020 15:00	Carbon Dioxide	115 ppm	44	04/29/21 15:00
CID12 GS1 (Prior to Leak Testing)				**CID12 GS2 (Post Leak Testing)**				**CID12 GS3 (Post Thermal Testing)**			
Analyte	Quantitation	AMU	Date	Analyte	Quantitation	AMU	Date	Analyte	Quantitation	AMU	Date
Hydrogen	85 ppm	2	12/11/2020 14:36	Hydrogen	55 ppm	2	12/11/2020 15:24	Hydrogen	82 ppm	2	05/11/2021 15:45
Helium	20.0%	4	12/11/2020 14:36	Helium	53.0%	4	12/11/2020 15:24	Helium	ND	4	05/11/2021 15:45
Water	365 ppm	18	12/11/2020 14:36	Water	0 ppm	18	12/11/2020 15:24	Water	1597 ppm	18	05/11/2021 15:45
Nitrogen	62.5%	28	12/11/2020 14:36	Nitrogen	36.4%	28	12/11/2020 15:24	Nitrogen	77.9%	28	05/11/2021 15:45
Oxygen	16.6%	32	12/11/2020 14:36	Oxygen	10.1%	32	12/11/2020 15:24	Oxygen	21.0%	32	05/11/2021 15:45
Argon	7930 ppm	40	12/11/2020 14:36	Argon	4572 ppm	40	12/11/2020 15:24	Argon	9341 ppm	40	05/11/2021 15:45
Carbon Dioxide	231 ppm	44	12/11/2020 14:36	Carbon Dioxide	160 ppm	44	12/11/2020 15:24	Carbon Dioxide	425 ppm	44	05/11/2021 15:45

Figure 7-2. Gas Sample Summary for CID8 - CID12

7.2. Illustrations of TC locations on Vessel, Shroud, and Pressure Manifold

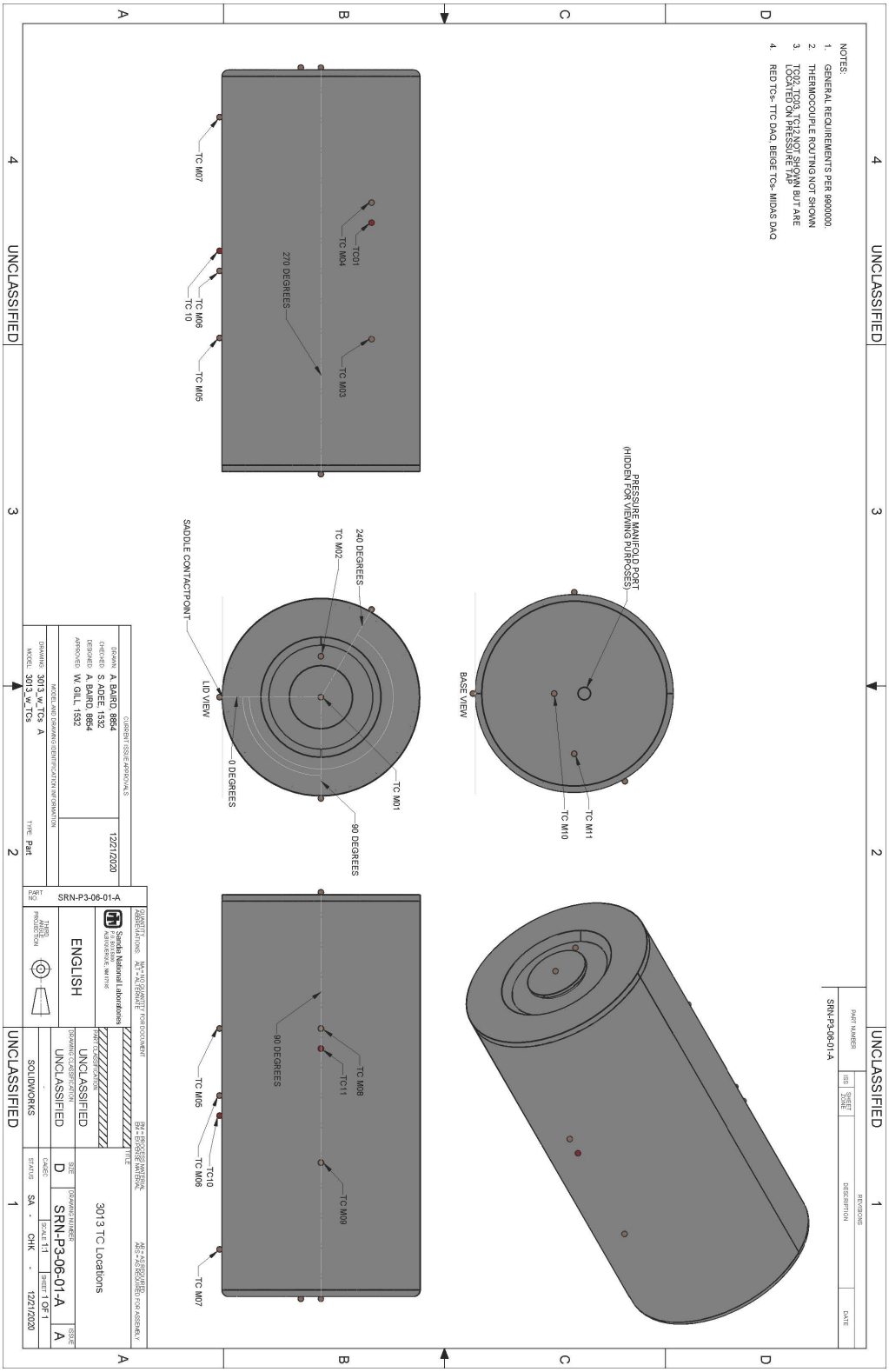

Figure 7-3. TC Locations on Vessel.

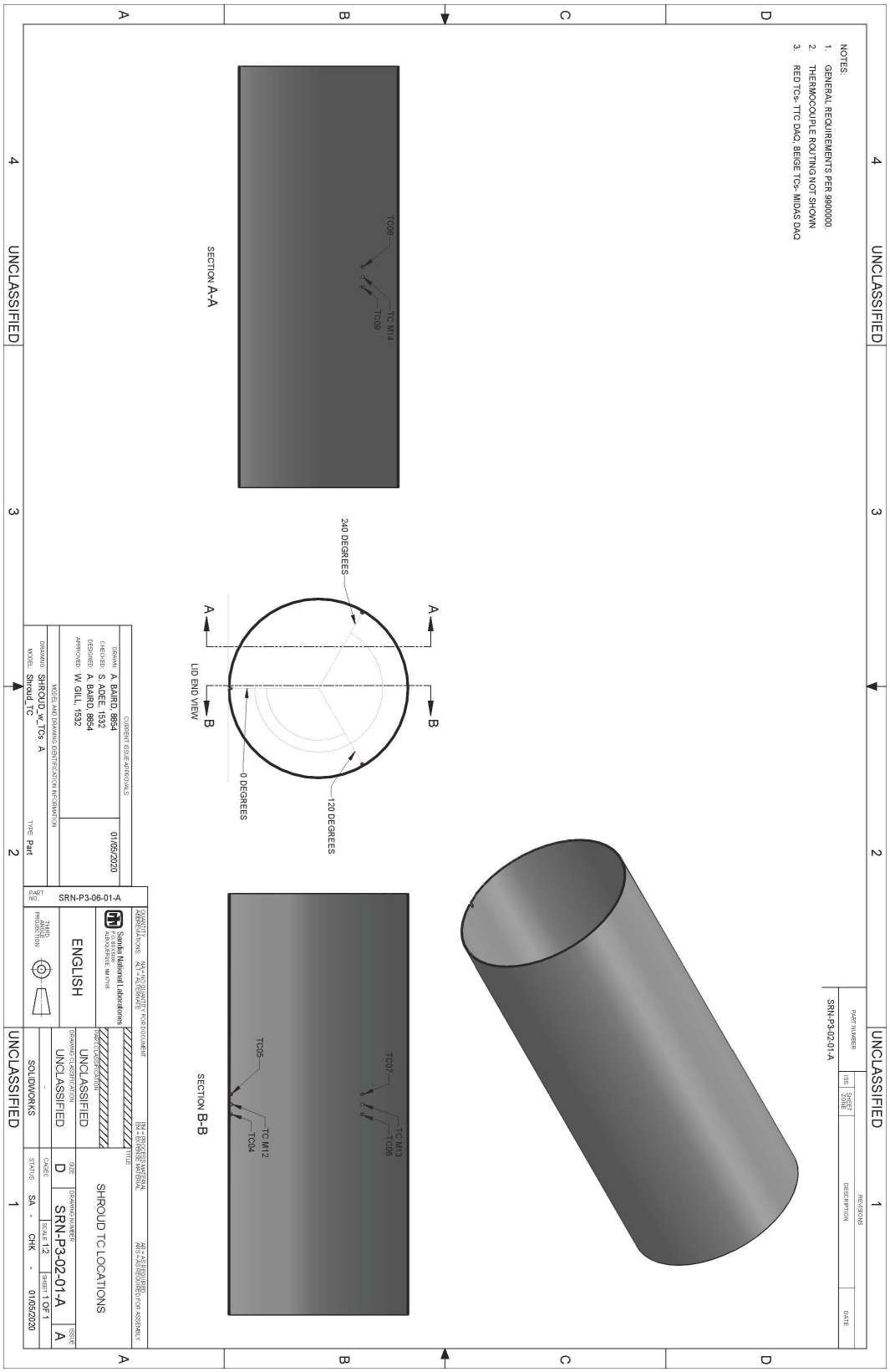

Figure 7-4. TC Locations on Shroud.

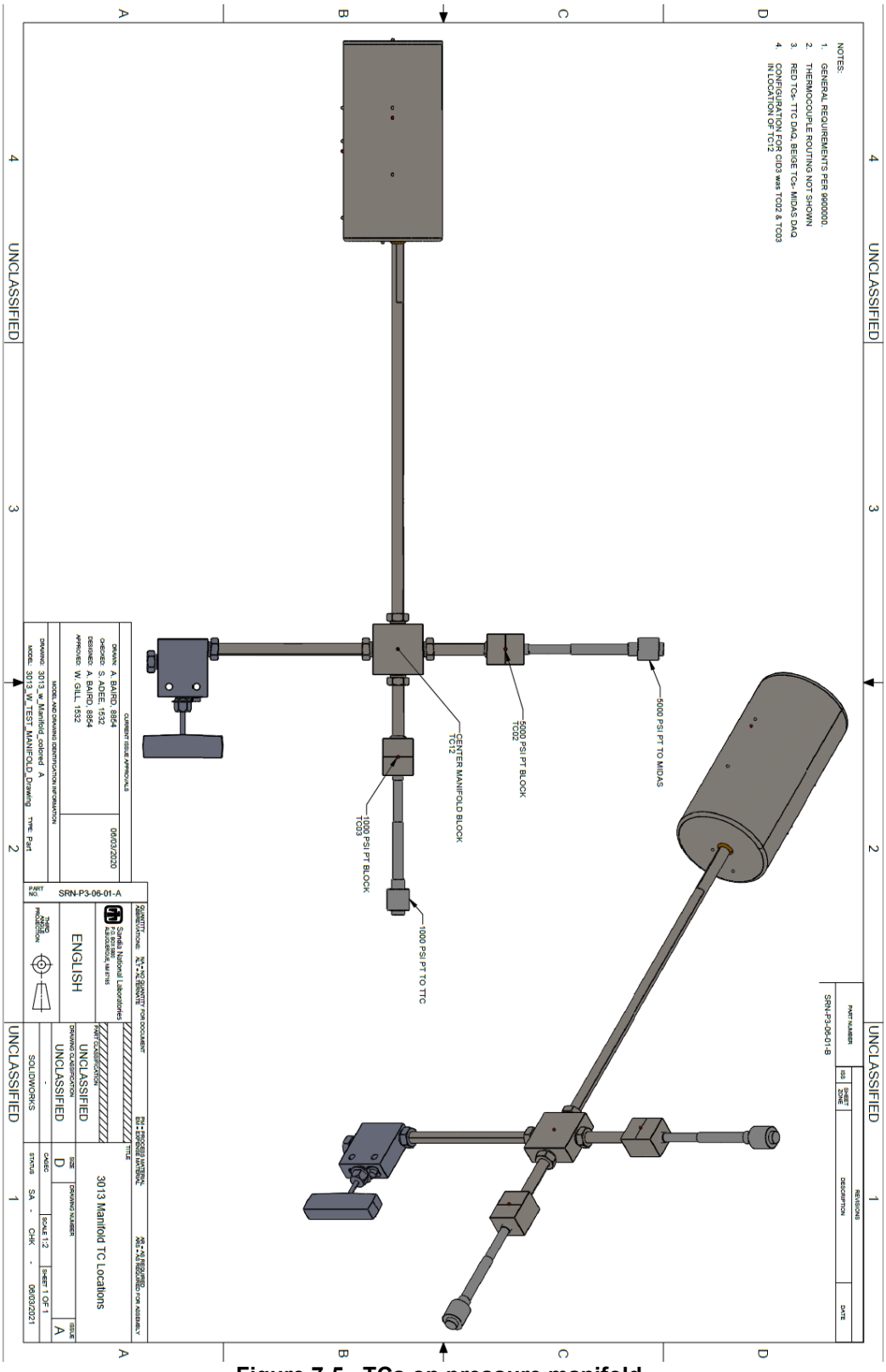

Figure 7-5. TCs on pressure manifold.

DISTRIBUTION

Email—Internal

Name	Org.	Sandia Email Address
Scott Sanborn	08854	sesanbo@sandia.gov
Carlos Lopez	01532	carlope@sandia.gov
Technical Library	01911	sanddocs@sandia.gov

Email—External [redacted]

Name	Company Email Address	Company Name
Hilda Coleman	hilda.coleman@srs.gov	Savannah River Site
Ray Sprankle	ray.sprankle@srs.gov	Savannah River Site
James McClard	james.mcclard@srs.gov	Savannah River Site
Steve Hensel	steve.hensel@srs.gov	Savannah River Site

This page left blank

This page left blank

Sandia National Laboratories

Sandia National Laboratories is a multimission laboratory managed and operated by National Technology & Engineering Solutions of Sandia LLC, a wholly owned subsidiary of Honeywell International Inc. for the U.S. Department of Energy's National Nuclear Security Administration under contract DE-NA0003525.